

# Caspase-7 activates ASM to repair gasdermin and perforin pores

<https://doi.org/10.1038/s41586-022-04825-8>

Received: 29 May 2019

Accepted: 29 April 2022

Published online: 15 June 2022

 Check for updates

Kengo Nozaki<sup>1,2,6</sup>, Vivien I. Maltez<sup>3,6</sup>, Manira Rayamajhi<sup>3</sup>, Alan L. Tubbs<sup>3</sup>, Joseph E. Mitchell<sup>3,4</sup>, Carolyn A. Lacey<sup>1,2</sup>, Carissa K. Harvest<sup>1,2,3</sup>, Lupeng Li<sup>1,2,3</sup>, William T. Nash<sup>5</sup>, Heather N. Larson<sup>1,2</sup>, Benjamin D. McGlaughon<sup>3</sup>, Nathaniel J. Moorman<sup>3</sup>, Michael G. Brown<sup>5</sup>, Jason K. Whitmire<sup>3,4</sup> & Edward A. Miao<sup>1,2,✉</sup>

Among the caspases that cause regulated cell death, a unique function for caspase-7 has remained elusive. Caspase-3 performs apoptosis, whereas caspase-7 is typically considered an inefficient back-up. Caspase-1 activates gasdermin D pores to lyse the cell; however, caspase-1 also activates caspase-7 for unknown reasons<sup>1</sup>. Caspases can also trigger cell-type-specific death responses; for example, caspase-1 causes the extrusion of intestinal epithelial cell (IECs) in response to infection with *Salmonella enterica* subsp. *enterica* serovar Typhimurium (*S. Typhimurium*)<sup>2,3</sup>. Here we show in both organoids and mice that caspase-7-deficient IECs do not complete extrusion. Mechanistically, caspase-7 counteracts gasdermin D pores and preserves cell integrity by cleaving and activating acid sphingomyelinase (ASM), which thereby generates copious amounts of ceramide to enable enhanced membrane repair. This provides time to complete the process of IEC extrusion. In parallel, we also show that caspase-7 and ASM cleavage are required to clear *Chromobacterium violaceum* and *Listeria monocytogenes* after perforin-pore-mediated attack by natural killer cells or cytotoxic T lymphocytes, which normally causes apoptosis in infected hepatocytes. Therefore, caspase-7 is not a conventional executioner but instead is a death facilitator that delays pore-driven lysis so that more-specialized processes, such as extrusion or apoptosis, can be completed before cell death. Cells must put their affairs in order before they die.

Caspase-3 is the primary apoptotic executioner, and is sufficient among caspases to cause apoptosis. By contrast, the roles of other executioners—such as caspase-7—remain unknown. Exemplifying this, *Casp3*<sup>-/-</sup> mice are perinatally lethal on the 129/SvJ background, whereas *Casp7*<sup>-/-</sup> mice are healthy<sup>4</sup>. However, on the C57BL/6 background, caspase-7 can rescue *Casp3*<sup>-/-</sup> mice<sup>5</sup>. This result leads to the present line of thinking that holds that caspase-7 is an inefficient back-up for caspase-3 that only works in certain conditions.

## Caspase-7 is required for IEC extrusion

Although caspase-7 is expressed in most tissues<sup>6</sup>, it is highly expressed in the intestine and in isolated IECs<sup>7</sup> (Extended Data Fig. 1a–c). After oral infection with *S. Typhimurium*, we observed many cleaved caspase-7-positive IECs in the caecum, all of which had a characteristic morphology that is indicative of ongoing extrusion into the lumen<sup>8</sup> (Extended Data Fig. 1d–f). Caspase-7 is classically known to be activated by apoptotic caspases, including caspase-3. However, infection did not increase cleaved-caspase-3-positive cells, and *Casp3*<sup>-/-</sup> mice retained increased levels of cleaved-caspase-7-positive cells (Extended Data Fig. 1g–i).

In wild-type mice, individual EpCAM<sup>+</sup> IECs extruded whereas neighbouring cells remained unperturbed in the monolayer during *S. Typhimurium* infection (Fig. 1a,b). Notably, in *Casp7*<sup>-/-</sup> mice, IECs extruded as clusters that remained attached to the apical epithelial surface (Fig. 1a,b). Clusters became marked 24 h after infection; in an extreme example, 18 IECs were observed in a single extrusion cluster site (Fig. 1b and Extended Data Fig. 1j–l). This clustered morphology has not to our knowledge been previously reported. Thus, caspase-7 is activated in extruding IECs in response to *S. Typhimurium* infection, but independently of the conventional apoptotic executioner caspase-3.

During *S. Typhimurium* infection, IEC extrusion is initiated when caspase-1 is activated by NAIP–NLRC4; this complex detects bacterial proteins, such as flagellin, in the cytosol<sup>2,3</sup>. This can be mimicked in IEC organoid cultures by stimulation with FlaTox, an engineered toxin that delivers flagellin to the cytosol, which causes extrusion in organoid monolayers in a setting in which all cells activate caspase-1. We therefore examined caspase-7 function in this model of IEC extrusion.

FlaTox-treated wild-type organoids ultimately collapse, concomitantly with the rupture of the inner contents into the surrounding matrigel. We visualized the morphology of extruding IECs, and in addition quantified organoid rupture as a proxy for overall extrusion

<sup>1</sup>Department of Immunology, Duke University School of Medicine, Durham, NC, USA. <sup>2</sup>Department of Molecular Genetics and Microbiology, Duke University School of Medicine, Durham, NC, USA. <sup>3</sup>Department of Microbiology and Immunology, University of North Carolina at Chapel Hill, Chapel Hill, NC, USA. <sup>4</sup>Department of Genetics, University of North Carolina at Chapel Hill, Chapel Hill, NC, USA. <sup>5</sup>Department of Medicine, Division of Nephrology and the Beirne B. Carter Center for Immunology Research, University of Virginia, Charlottesville, VA, USA. <sup>6</sup>These authors contributed equally: Kengo Nozaki, Vivien I. Maltez. <sup>✉</sup>e-mail: edward.miao@duke.edu

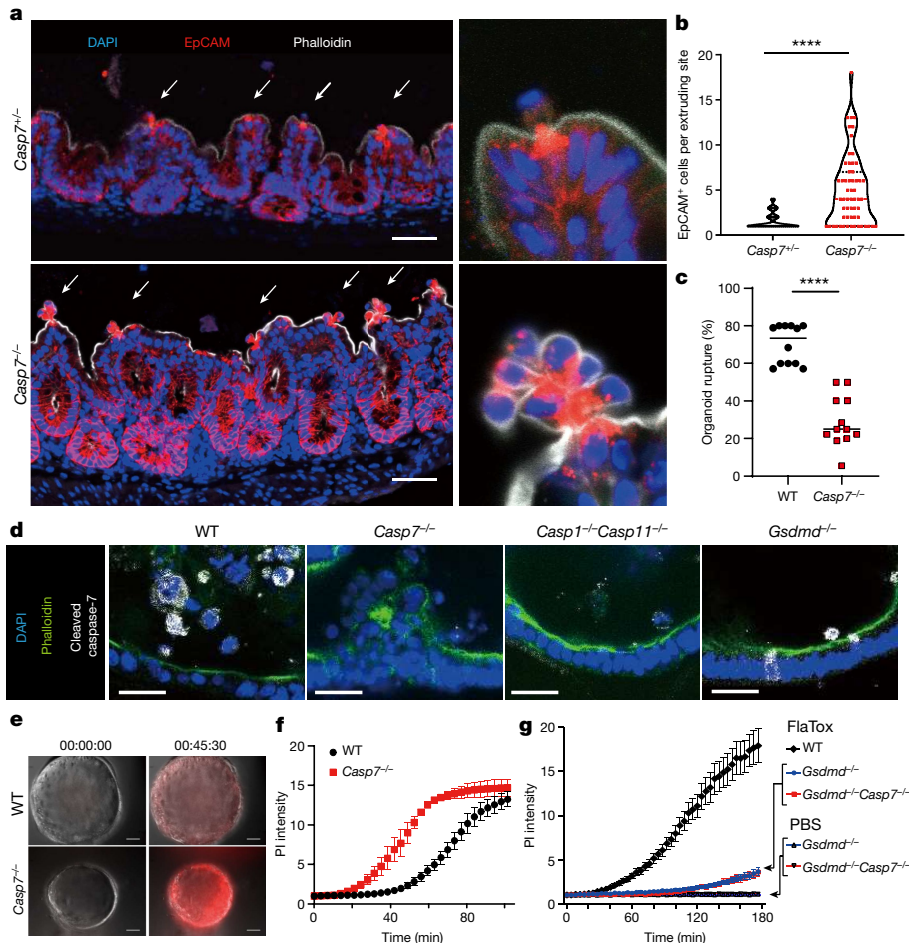


**Fig. 1 | Caspase-7 facilitates IEC extrusion during *S. Typhimurium* infection and ameliorates gasdermin D pores.** **a,b**, The indicated mice were infected with  $5 \times 10^6$  *S. Typhimurium* and the caeca were collected 24 h later. Representative images (**a**) and quantification (**b**) of epithelial marker EpCAM<sup>+</sup> cell counts per extrusion site (arrows indicate extrusion sites). WT, wild type. **c**, Percentage of ruptured IEC organoids after treatment with FlaTox in pooled live-imaging experiments (related to Extended Data Fig. 2a). **d**, Representative images of organoids 30 min after treatment with FlaTox, stained with phalloidin and for cleaved caspase-7. **e,f**, Representative images (**e**; full series

are in Extended Data Fig. 4b) and quantification (**f**) in live-cell imaging of PI intensity of wild-type and *Casp7*<sup>-/-</sup> organoids treated with FlaTox. **g**, PI Intensity of wild-type, *Gsdmd*<sup>-/-</sup> and *Gsdmd*<sup>-/-</sup>*Casp7*<sup>-/-</sup> organoids treated with FlaTox or control PBS. Data are representative of three experiments (**a,b,d-f**) or are pooled from 12 (**c**) or 3 (**g**) experiments. Scale bars, 50  $\mu$ m (**a**); 20  $\mu$ m (**d**). \* $P < 0.05$ , \*\* $P < 0.01$ , \*\*\* $P < 0.001$ , \*\*\*\* $P < 0.0001$  (two-sided Mann-Whitney U-test in **b**; two-sided unpaired t-test in **c**; two-way analysis of variance (ANOVA) with Sidak's post-hoc test in **f** or with Tukey's post-hoc test in **g**). Data are median  $\pm$  s.e.m. (**b**) or mean  $\pm$  s.e.m. (**c,f,g**). Exact  $P$  values in Source Data.

dynamics. In *Casp7*<sup>-/-</sup> organoids, the IECs also initiated extrusion; however, they remained attached to neighbouring IECs, formed clusters of defectively extruding cells and ultimately had a reduced incidence of organoid rupture (Supplementary Videos 1,2, Fig. 1c and Extended Data Fig. 2a,b). *Casp3*<sup>-/-</sup> organoids retained normal levels of extrusion, cleaved caspase-7 and rupture (Extended Data Fig. 2c–e). Therefore, caspase-7 is critical for the caspase-1-driven extrusion of IECs, and this occurs independently of caspase-3.

### Caspase-1 activates caspase-7

Caspase-1 is an inflammatory caspase that is highly expressed in IECs<sup>7</sup> (Extended Data Fig. 1c). Caspase-1 can cleave and activate caspase-7, although the physiological relevance of this remains unknown<sup>1</sup>. We also observed this cleavage in IEC organoids; caspase-7 was cleaved as early as 15–30 min after treatment with FlaTox, concomitantly with caspase-1 cleavage. This cleaved caspase-7 staining was lost in *Casp1*<sup>-/-</sup>*Casp11*<sup>-/-</sup> organoids (*Casp11* is also known as *Casp4*), as shown by the delayed cleavage kinetics in western blotting experiments, but remained present in IECs that lack gasdermin D (*Gsdmd*<sup>-/-</sup> IECs) (Fig. 1d and Extended Data Fig. 2f). By contrast, cleavage of caspase-3 was not observed in the first 30 min,

and *Casp3*<sup>-/-</sup> organoids retained staining for cleaved caspase-7; only after 45 min in *Casp1*<sup>-/-</sup>*Casp11*<sup>-/-</sup> organoids did we observe the cleavage of apoptotic caspase-8, caspase-9 and caspase-3 (Extended Data Fig. 2e,f). This suggests that secondary pathways (for example, ASC–caspase-8 (ref.<sup>9</sup>)) can activate both caspase-3 and caspase-7, but with delayed kinetics. This salvage pathway is slower than caspase-1, which rapidly activates caspase-7 after NLRP4 stimulation.

### Caspase-7 antagonizes gasdermin D

Caspase-1 also cleaves gasdermin D, which forms pores in the plasma membrane<sup>9</sup>. Both gasdermin D and caspase-7 are cleaved 15 min after treatment with FlaTox, independently of one another (Extended Data Figs. 2f and 3a). However, gasdermin pore permeability, as assessed by propidium iodide (PI) uptake, was accelerated in *Casp7*<sup>-/-</sup> organoids, (Supplementary Videos 3,4,7 and 8, Fig. 1e,f and Extended Data Fig. 3b,c). This caspase-7 effect was not seen during apoptosis activated by tumour necrosis factor (TNF) with cycloheximide (CHX) or by the caspase-1–BID pathway that occurs in *Gsdmd*<sup>-/-</sup> cells<sup>9</sup> (Extended Data Fig. 3d and Fig. 1g). Identical conclusions were drawn using calcein-AM, which stains intact cells (Supplementary Videos 5,6,

# Article

Extended Data Fig. 3e,f). *Casp3*<sup>-/-</sup> organoids did not show this accelerated membrane permeability (Extended Data Fig. 3g,h). These results indicate that caspase-7 uniquely impedes the functionality of gasdermin D pores.

## ASM is cleaved by caspase-7

When the plasma membrane is damaged, cells have at least four mechanisms to repair the membrane: ASM-driven endocytosis; ESCRT-induced shedding; constriction; and patching<sup>10</sup>. Among these, ASM is a sphingomyelin-converting enzyme that is located inside the lysosome. Once the plasma membrane is damaged, Ca<sup>2+</sup> triggers lysosomal exocytosis into the damaged site, where the released ASM can repair the plasma membrane<sup>10</sup>. In studies unrelated to membrane repair, caspase-7 was found to cleave ASM and enhance sphingomyelin-catalysing activity<sup>11</sup>. Despite this link to ASM, a role for caspase-7 in membrane repair has not to our knowledge been investigated previously. We hypothesized that the caspase-7-dependent antagonization of the gasdermin D pore that we observed (Fig. 1e–g) resulted from caspase-7 cleaving and activating ASM.

Full-length ASM (pro-ASM; a 72-kDa band) is cleaved by caspase-7 to generate a 57-kDa form with greater enzymatic activity<sup>11</sup>. In resting organoids, the pro-ASM band is dominant, but treatment with FlaTox causes the cleaved band to appear in wild-type organoids (Extended Data Fig. 4a–c). The immunoreactivity of cleaved ASM is stronger than that of pro-ASM—an effect that is also seen with the anti-gasdermin D antibody (Extended Data Fig. 3a), albeit to a lesser degree. ASM cleavage required caspase-7, and in addition NLRC4 and caspase-1, but not caspase-3 (Extended Data Fig. 4b,c). We observed that the 57-kDa cleaved form of ASM was glycosylated, consistent with this band being an active enzyme<sup>12</sup> (Extended Data Fig. 4d). Thus, caspase-7 specifically cleaves ASM in our organoid model.

## Caspase-7-activated ASM makes ceramide

Sphingomyelin is a major constituent of the membrane in animal cells, and contains a head group that is attached to two lipid groups. The sphingomyelin head group allows the plasma membrane to remain largely flat. ASM removes the head group of sphingomyelin, converting it into ceramide. Ceramide causes the membrane to naturally invaginate, which causes spontaneous clathrin-independent endocytosis that internalizes proteinaceous pores in the plasma membrane (Extended Data Fig. 5a). This endocytosis repairs membrane damage quickly—streptolysin O pores are repaired within 30 s (ref. <sup>13</sup>). We hypothesized that by activating ASM to produce ceramide, caspase-7 would enhance endocytic membrane repair of the gasdermin D pore.

We found that infection with *S. Typhimurium* resulted in strong ceramide staining in extruding IECs, but not in neighbouring IECs (Fig. 2a and Extended Data Fig. 5b,c). By contrast, *Casp7*<sup>-/-</sup> mice had no ceramide enrichment in the abnormal IEC extrusion clusters (Fig. 2a). Organoids showed the same caspase-7-dependent ceramide production after treatment with FlaTox (Extended Data Fig. 5d–f). By contrast, organoids that were treated with a functional inhibitor of ASM, imipramine (IMP)<sup>14</sup>, lost ceramide staining but retained caspase-7 cleavage (Extended Data Fig. 5d–f). Wild-type organoids that were treated with IMP had a significantly reduced incidence of rupture, showed more rapid PI entry and calcein loss and had a faster extrusion initiation time, all similar to *Casp7*<sup>-/-</sup> organoids (Fig. 2b,c and Extended Data Fig. 5g,h). By contrast, wild-type and *Casp3*<sup>-/-</sup> organoids initiated extrusion at similar times (Extended Data Fig. 5i). Finally, treatment with ceramide normalized the PI staining, extrusion initiation time and rupture percentage in *Casp7*<sup>-/-</sup> organoids (Extended Data Fig. 5j–l).

We next applied IMP treatments to our *S. Typhimurium* infection *in vivo*. Similar to *Casp7*<sup>-/-</sup> mice, IMP-treated wild-type mice showed

abnormal extrusion clusters (Fig. 2d), and in addition contained cleaved-caspase-7-positive IECs that did not exhibit the morphology of extrusion (Extended Data Fig. 5m). This could be the result of impairment very early in the extrusion process. Furthermore, treatment with IMP did not prevent cleaved caspase-7 staining in the extruding clusters, but ceramide staining was lost (Fig. 2e). We also found the abnormal extruding clusters in IMP-treated organoids after stimulation with FlaTox (Extended Data Fig. 5n). Consistent with caspase-1-activating caspase-7, ceramide staining was lost in *Casp1*<sup>-/-</sup> *Casp11*<sup>-/-</sup> mice (Fig. 2e). Altogether, these data indicate that caspase-7 activates ASM to generate ceramide, which can reseal gasdermin D pores in extruding IECs. Moreover, depletion of ASM causes defective IEC extrusion clusters, similar to the phenotype that is observed with caspase-7 deficiency.

## Gasdermin D links caspase-7 to ceramide

The above data strongly associate caspase-7 and ASM. However, ASM resides in the lysosomal lumen, whereas caspase-7 resides in the cytosol, and how caspase-7 crosses the membrane to interact with and cleave ASM remains unclear. We hypothesized that the gasdermin D pore was the conduit. Consistent with this, in FlaTox-treated *Gsdmd*<sup>-/-</sup> organoids, caspase-7 was activated, but was unable to cleave ASM (Extended Data Figs. 2f and 4b). Furthermore, ceramide production was lost in *Gsdmd*<sup>-/-</sup> mice during infection (Fig. 2e and Extended Data Fig. 6). These data support the hypothesis that caspase-7 passes through the gasdermin D pore to encounter and cleave ASM; notably, these are the same pores that require ASM-driven membrane repair.

## Cleaved ASM repairs membranes

IMP affects many lysosomal proteins, and is thus not fully specific to ASM. To specifically eliminate the caspase-7 cleavage site in ASM, we generated ASM(D249A) (*Smpd1*<sup>DA/DA</sup>) mice by CRISPR–Cas9 mutagenesis (Extended Data Fig. 7a). *Smpd1*<sup>DA/DA</sup> mice were fertile and healthy to at least five months of age. During infection with *S. Typhimurium*, *Smpd1*<sup>DA/DA</sup> mice showed the same extrusion defect as *Casp7*<sup>-/-</sup> mice (Fig. 3a, and Extended Data Fig. 7b). As in IMP-treated mice, caspase-7 was activated in the extruding cell clusters in *Smpd1*<sup>DA/DA</sup> mice (Fig. 3c), and *Smpd1*<sup>DA/DA</sup> organoids that were treated with FlaTox (but not those that were treated with TNF + CHX) showed faster PI uptake, reduced rupture incidence and faster extrusion initiation (Fig. 3d, Supplementary Video 9 and Extended Data Fig. 7c–f). Of note, *Smpd1*<sup>DA/DA</sup> organoids that were treated with FlaTox showed no ASM cleavage (Fig. 3e). Therefore, mice that are resistant to caspase-7 cleavage replicate the phenotypes that are seen in *Casp7*<sup>-/-</sup> mice and IMP-treated mice.

## Caspase-7 mitigates intestinal pathology

Wild-type mice show considerable intestinal pathology during infection with *S. Typhimurium*, whereas *Casp1*<sup>-/-</sup> *Casp11*<sup>-/-</sup> mice exhibit minimal pathology<sup>15</sup>. By contrast, *Casp7*<sup>-/-</sup> mice showed worsened pathology and cytokine response, with extruded cells retained in proximity to the gut wall 48 h after infection (Extended Data Fig. 8a–d). However, bacterial burdens were minimally altered in *Casp7*<sup>-/-</sup> or *Smpd1*<sup>DA/DA</sup> mice (Extended Data Fig. 8e–j). We observed similar results during dextran sodium sulfate (DSS)-induced colitis, in which *Casp7*<sup>-/-</sup> mice showed exacerbated weight loss and pathology (Extended Data Fig. 8k–l). Thus, caspase-7 is important for reducing intestinal damage, but not for reducing the *S. Typhimurium* burden.

These results indicate that a series of events is required to facilitate IEC extrusion downstream of caspase-1: caspase-7 passes through gasdermin D pores, then cleaves ASM, potentiating its activity to generate ceramide, which mediates membrane repair to ensure that extrusion

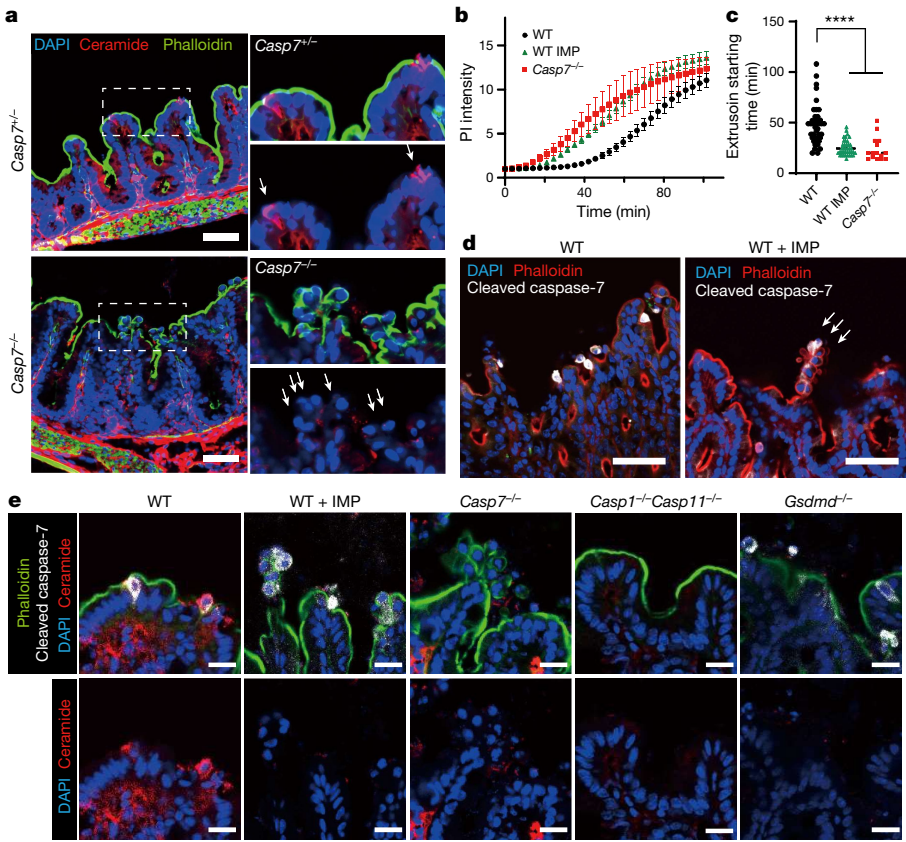


**Fig. 2 | Caspase-7 activation drives ASM to repair gasdermin D pores and facilitate IEC extrusion.** **a**, The indicated mice were infected with  $5 \times 10^6$  *S. Typhimurium* and the caeca were collected 24 h later. Ceramide staining; dotted rectangles are shown at a higher magnification on the right (arrows indicate individual extruding cells). **b,c**, The indicated organoids treated with FlaxTox were live-imaged, and the PI intensity (**b**) or extrusion starting time (**c**) were quantified. **d,e**, The indicated mice were infected with  $5 \times 10^6$  *S. Typhimurium* and the caeca were collected 24 h later. **d**, Cleaved caspase-7

staining (arrows indicate extruding cell clusters). **e**, Ceramide and cleaved caspase-7 staining. Scale bars, 50  $\mu\text{m}$  (**a,d**); 20  $\mu\text{m}$  (**e**). Data are representative of three experiments (**a,d,e**) or are pooled from three experiments (**b,c**). For **c**, WT  $n = 41$ , WT + IMP  $n = 39$  and *Casp7*<sup>-/-</sup>  $n = 15$  organoids pooled from three experiments were analysed. \* $P < 0.05$ , \*\* $P < 0.01$ , \*\*\* $P < 0.001$ , \*\*\*\* $P < 0.0001$  (two-way ANOVA with Tukey's post-hoc test in **b**; one-way ANOVA with Tukey's post-hoc test in **c**). Data are mean  $\pm$  s.e.m. Exact  $P$  values in Source Data.

completes successfully. Defective extrusion causes pathology, but does not reverse bacterial burdens.

If activating ASM is the core evolved function of caspase-7, then this should hold true in other model systems in which cell death involves pores concomitantly with the activation of caspase-7. The most classical example of this is the perforin pore attack pathway that is used by natural killer (NK) cells and cytotoxic T lymphocytes (CTLs) to activate apoptosis.

## NK cell perforin defence requires caspase-7

NK cells and CTLs use perforin pores to deliver granzyme B, which activates all three of the apoptotic executioner caspases: caspase-3 (refs. <sup>16,17</sup>), caspase-7 (refs. <sup>18,19</sup>) and caspase-6 (ref. <sup>20</sup>). NK cells and CTLs attack host cells that contain intracellular pathogens, which eliminates the infected cells<sup>21</sup>. Notably, perforin pores are similar in size to gasdermin pores. However, a unique role for caspase-7 after perforin-mediated attack remains elusive.

We discovered a model pathogen, *Chromobacterium violaceum*, in which NK cell perforin attack clears bacteria. *C. violaceum* is a ubiquitous environmental bacterium that only infects immunocompromised individuals<sup>22</sup>. The immune system actually uses both apoptosis and pyroptosis to combat *C. violaceum*; each is required in a different cell type<sup>23</sup>. Pyroptosis is implicated in the clearance of bacteria from the spleen, in which NLRC4 and caspase-1 are essential probably in macrophages, but the caspase-1-processed cytokines IL-1 $\beta$  and IL-18 are dispensable<sup>23</sup>.

In the liver there is an additional role for IL-18, which primes NK cells to use perforin attack on hepatocytes (in which caspase-1 is not detectable)<sup>23</sup>.

*Casp7*<sup>-/-</sup> mice, but not *Casp6*<sup>-/-</sup> mice, were more susceptible to infection with *C. violaceum*, phenocopying *Prf1*<sup>-/-</sup> mice (Fig. 4a,b and Extended Data Fig. 9a,b). Thus, we discovered another *in vivo* phenotype with which to study caspase-7. We expected that *Casp3*<sup>-/-</sup> mice, which lack the primary apoptotic executioner, would be susceptible to *C. violaceum*. Instead, *Casp3*<sup>-/-</sup> mice were aberrantly hyper-resistant (Extended Data Fig. 9a). This does not indicate that caspase-3 enhances infection; *Casp3*<sup>-/-</sup> mice are known to have an abnormal immune system. Our results may be another example of the aberrant tonic type I interferon (IFN) signalling that is seen in caspase-3-deficient mice, which causes aberrant resistance to viruses<sup>24,25</sup>. *Casp7*<sup>-/-</sup> and *Casp6*<sup>-/-</sup> mice do not suffer from this caveat. Thus, although caspase-3 is fully sufficient to accomplish apoptosis *in vitro*, caspase-3 is unable to compensate for the loss of caspase-7 in defence against *C. violaceum* *in vivo*.

## Caspase-7 acts in hepatocytes

NLRC4-driven IL-18 is upstream of NK cell perforin during *C. violaceum* infection<sup>23</sup>. IL-18 therapy rescued *Nlrc4*<sup>-/-</sup> mice, but not *Casp7*<sup>-/-</sup> mice (Fig. 4c) or *Prf1*<sup>-/-</sup> mice<sup>23</sup>. Furthermore, liver burdens in *Casp7*<sup>-/-</sup> mice and *Prf1*<sup>-/-</sup> mice were comparable (Fig. 4b and Extended Data Fig. 9b), which suggests that there is a common defence pathway. Using NK cell adoptive transfer, we determined that perforin acted in NK cells,

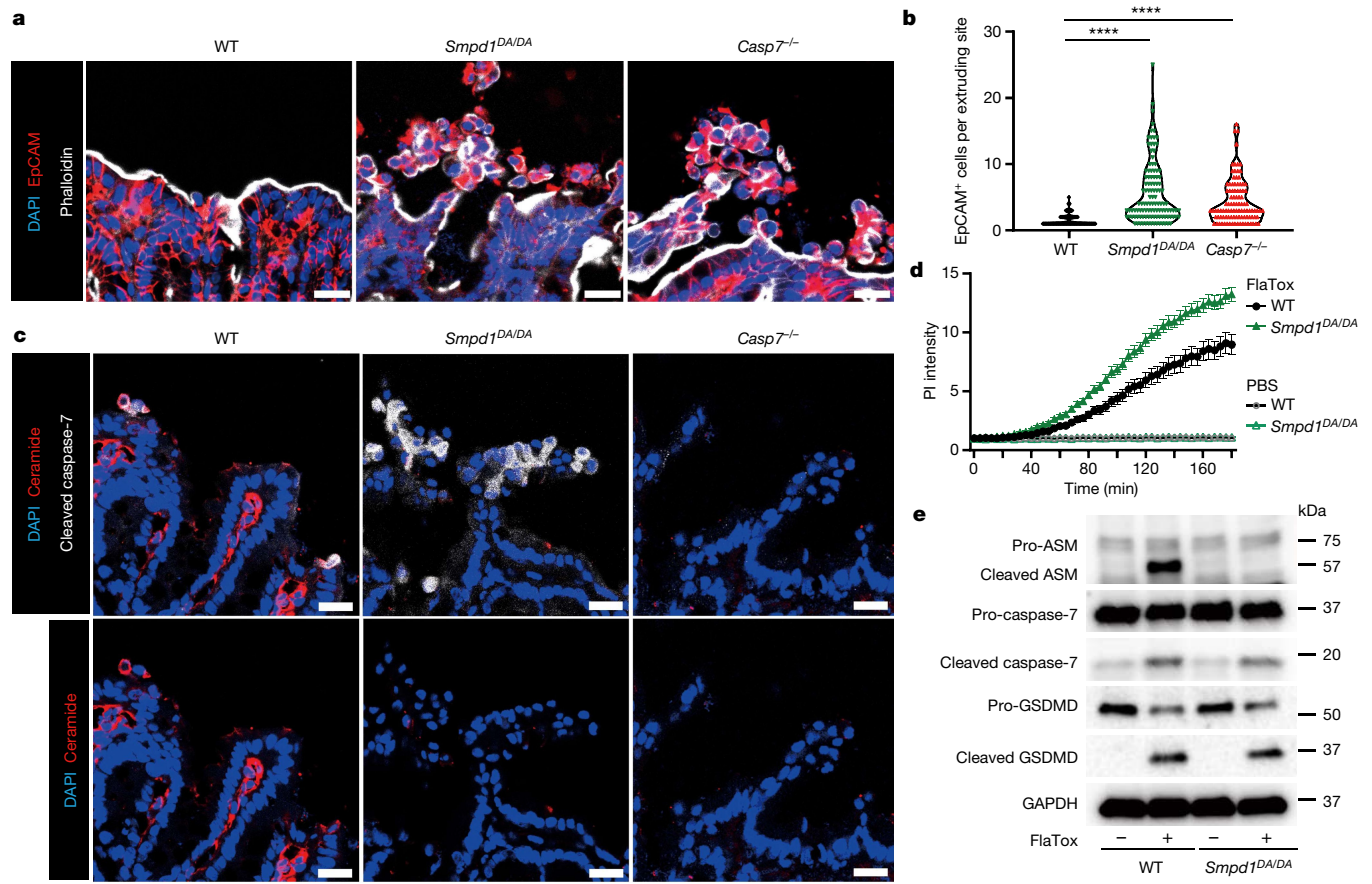


**Fig. 3 | A mutation in ASM that renders ASM resistant to cleavage impairs membrane repair and IEC extrusion.** **a–c**, The indicated mice were infected with  $5 \times 10^6$  S. Typhimurium and the caeca were collected 24 h later. Representative images (a) and quantification (b) of EpCAM<sup>+</sup> cell counts per extruding site. **c**, Ceramide and cleaved caspase-7 staining. **d**, The indicated organoids treated with FlaTox or PBS control were live-imaged, and the PI intensity was quantified. **e**, The indicated organoids were removed of dead

cells and then stimulated for 20 min with PBS or FlaTox, and the cleavage of ASM, caspase-7 and GSDMD was assessed. Data are representative of three experiments (a–c,e) or are pooled from three experiments (d). Scale bars, 20  $\mu$ m. \* $P < 0.05$ , \*\* $P < 0.01$ , \*\*\* $P < 0.001$ , \*\*\*\* $P < 0.0001$  (two-sided Mann–Whitney U-test in b; two-way ANOVA with Sidak's post-hoc test in d). Data are median  $\pm$  s.e.m. (b) or mean  $\pm$  s.e.m. (d). Exact P values in Source Data.

whereas caspase-7 did not (Fig. 4d,e and Extended Data Fig. 9c,d). Thus, caspase-7 acts downstream of both IL-18 and NK cell perforin to defend the liver from infection with *C. violaceum*.

We previously showed that *C. violaceum* is located in hepatocytes<sup>23</sup>, and thus we hypothesized that hepatocytes would contain activated caspase-7. To synchronize NK cell attack and downstream caspase-7 activation, we used IL-18 therapy in *Casp1<sup>-/-</sup>*/*Casp11<sup>-/-</sup>* mice. *C. violaceum* liver infection results in macroscopic 2-to-3-mm lesions<sup>23</sup> that are identifiable by DAPI staining, in which cleaved caspase-7 was visualized in hepatocytes (marked by CPS1) (Fig. 4f and Extended Data Fig. 10a–d). Cleaved caspase-3 and cleaved caspase-7 were both observed in serial sections, and cleaved caspase-3 remained present in *Casp7<sup>-/-</sup>* mice; in addition, these cells were positive for a marker of apoptosis (TUNEL) (Extended Data Fig. 10e–j). Cleaved caspase-7 and cleaved PARP (another apoptosis marker) were also observed in wild-type mice (Extended Data Fig. 10k,l). Therefore, apoptotic caspase-7 and caspase-3 are both activated in hepatocytes, in which caspase-7 has an essential role that cannot be compensated for by caspase-3.

### Caspase-7 activates ASM after NK cell attack

One feature in common between the *Salmonella*–IEC model and the *C. violaceum*–hepatocyte model is that both require caspase-7 and form plasma membrane pores during the cell death processes. We hypothesized that caspase-7-amplified ASM activity could explain

its role downstream of NK cell perforin attack. Depletion of ASM in wild-type mice caused an increase in the burden of *C. violaceum* in wild-type mice, but not in *Casp7<sup>-/-</sup>* mice (Fig. 4g). In infected livers, ceramide staining became intense around the inflammatory foci, encircling the lesion within cleaved-caspase-7-positive cells in wild-type mice, but not in *Casp7<sup>-/-</sup>* or IMP-treated mice (Extended Data Fig. 11). The few ceramide-positive cells after treatment with IMP may have escaped complete ASM depletion. We also infected *Smpd1<sup>DA/DA</sup>* mice with *C. violaceum* and found increased burdens and decreased ceramide staining, similar to *Casp7<sup>-/-</sup>* and IMP-treated wild-type mice (Fig. 4h,i). These data suggest that several key events are required for the clearance of *C. violaceum*: NK cell perforin attack, caspase-7 cleavage, ASM cleavage and ceramide production.

### NK cells clear *Listeria* through caspase-7

*Listeria monocytogenes* is useful to compare to *C. violaceum* because both are tropic for hepatocytes (Extended Data Fig. 12a). However, unlike *C. violaceum*, *L. monocytogenes* evades inflammasomes in vivo<sup>26,27</sup>, limiting IL-18 release<sup>28</sup> to a level that avoids priming the host NK cytotoxic response. In line with this, wild-type and *Casp7<sup>-/-</sup>* mice have equal burdens three days after infection. This susceptibility was corrected with IL-18 therapy in wild-type mice, which was not successful in NK-cell-depleted mice, *Casp7<sup>-/-</sup>* mice (Extended Data Fig. 12b,c) or *Prf1<sup>-/-</sup>* mice<sup>23</sup>, matching our results with

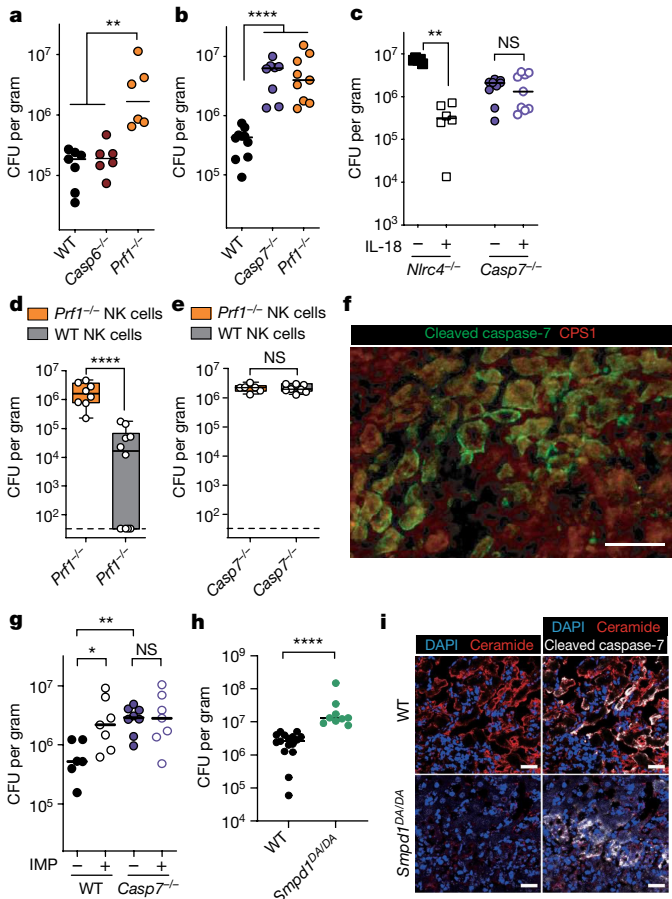


**Fig. 4 | NK cell perforin attack cleaves caspase-7 and ASM to clear *C. violaceum*.** **a–i.** The indicated mice were infected with  $10^2$  (c) or  $10^4$  (a,b,d–i) *C. violaceum*. **a–e,g,h.** Enumeration of liver burdens at three days post-infection (dpi). CFU, colony-forming units. **c,f.** Mice were treated with recombinant IL-18 or PBS control (day 0 and 1). **d,e.** Mice were adoptively transferred with NK cells from the indicated sources 24 h before infection. **f.** Livers were stained for the indicated markers by immunofluorescence at 2 dpi. Scale bar, 50  $\mu$ m. A larger image area and single channels are shown in Extended Data Fig. 8b. **g,h.** Mice were treated with IMP or PBS. **i.** Representative images of infected livers at 3 dpi stained for the indicated markers. Scale bars, 20  $\mu$ m. Data are pooled from two experiments (a–e) or from three experiments (g,h), or are representative of two experiments (f,i). Mouse numbers: **a, WT**  $n=7$ , **Casp6<sup>-/-</sup>**  $n=6$ , **Prf1<sup>-/-</sup>**  $n=6$ ; **b, WT**  $n=10$ , **Casp7<sup>-/-</sup>**  $n=7$ , **Prf1<sup>-/-</sup>**  $n=8$ ; **c, PBS**-treated  $n=6$  and IL-18-treated  $n=6$  **Nlrc4<sup>-/-</sup>**; **Casp7<sup>-/-</sup>**  $n=9$  each; **d, Prf1<sup>-/-</sup>**  $n=9$ , **Casp7<sup>-/-</sup>**  $n=7$ ; **g, WT**  $n=6$ , **WT** IMP  $n=7$ , **Casp7<sup>-/-</sup>** control  $n=8$ , **Casp7<sup>-/-</sup>** IMP  $n=7$ ; **h, WT**  $n=16$ , **Smpd1<sup>DA/DA</sup>**  $n=9$ . \* $P < 0.05$ , \*\* $P < 0.01$ , \*\*\* $P < 0.001$ , \*\*\*\* $P < 0.0001$ ; NS, not significant (two-sided Mann–Whitney U-test in a–e,h; one-way ANOVA in g). Bars indicate median values. Box plots show median and 25th–75th percentiles; whiskers are minimum and maximum values. Exact  $P$  values in Source Data.

*C. violaceum*. Therefore, IL-18 primes NK cell cytotoxicity to clear a Gram-negative and a Gram-positive intracellular bacterium, both requiring caspase-7.

### CTLs clear *Listeria* through caspase-7

Although *L. monocytogenes* evades NK cell cytotoxicity during a natural infection, it is efficiently identified and eradicated by the CTL response. CTL perforin attack during *L. monocytogenes* infection is typically studied using adoptive transfer experiments, which minimizes redundancy from the responses of T helper 1 cells<sup>29,30</sup> (Extended Data Fig. 12d–k). As a control, naive CTL transfer resulted

in the expected high burdens in both wild-type and *Casp7<sup>-/-</sup>* mice. Immune CTLs from vaccinated mice reduced burdens in wild-type (or *Casp6<sup>-/-</sup>*) mice, but were significantly defective in *Casp7<sup>-/-</sup>* recipients (Fig. 5a and Extended Data Fig. 12l). Perforin was required in CTLs whereas caspase-7 was required in the recipient mouse (Fig. 5b,c). Finally, when we compared *Prf1<sup>-/-</sup>* CTLs in a wild-type recipient (an effective single perforin knockout) to *Prf1<sup>-/-</sup>* CTLs in a *Casp7<sup>-/-</sup>* recipient (which should be an effective double knockout), there was no additive effect (Extended Data Fig. 12m). The residual clearance in *Casp7<sup>-/-</sup>* mice was mostly dependent on IFN $\gamma$  (Extended Data Fig. 12n), as expected.

Cleaved-caspase-7-positive hepatocytes appeared specifically after immune CTL transfer, assessed by flow cytometry and histological staining within infected foci (Extended Data Fig. 13a–g). A large percentage of cleaved caspase-7-positive cells had identifiable *L. monocytogenes* (Extended Data Fig. 13h,i). Thus, perforin activity is required in CTLs, whereas caspase-7 activity is required in hepatocytes.

### Caspase-7 activates ASM after CTL attack

Again, we hypothesized that the mechanism of caspase-7 function was through activation of ASM. IMP-treated wild-type mice showed increased *L. monocytogenes* burdens after immune CTL transfer, but again IMP treatment did not affect burdens in *Casp7<sup>-/-</sup>* mice (Fig. 5d). Furthermore, *Smpd1<sup>DA/DA</sup>* mice also showed increased burdens (Fig. 5e). Thus, caspase-7 cleaves ASM so as to facilitate *L. monocytogenes* clearance after CTL attack.

Therefore, after NK cell or CTL attack, caspase-7 cleaves and activates ASM; this drives the production of ceramide, which is required for the eventual clearance of *C. violaceum* and *L. monocytogenes*.

### Caspase-7 is dispensable in some cases

Amongst viral infections, mouse cytomegalovirus (MCMV) and lymphocytic choriomeningitis virus (LCMV) are common models to study perforin defence after NK cell and CTL attack, respectively<sup>31,32</sup>. Although perforin is important for both, caspase-7 and caspase-6 were not (Extended Data Fig. 14). That caspase-7 was required for resistance against two bacteria but not two viruses might indicate direct bactericidal effects of caspase-7; however, we found no evidence for this (Extended Data Fig. 15). Thus, the role of caspase-7 depends on the nature of the infecting pathogen.

### Caspase-7 is dispensable for pyroptosis

During *C. violaceum* infection, we previously proposed that there are at least two niches defended by different cell death modalities: hepatocytes cleared by apoptosis; and macrophages cleared by pyroptosis. This raises the question of whether direct cleavage of caspase-7 by caspase-1 might also be important to clear *C. violaceum* in the spleen, where pyroptosis is likely to defend the niche. We found that *Gsdmd<sup>-/-</sup>* mice were susceptible and had spleen burdens equivalent to *Casp1<sup>-/-</sup>* *Casp11<sup>-/-</sup>* mice, but that *Casp7<sup>-/-</sup>* mice (and other genotypes studied herein) competently cleared their spleens (Extended Data Fig. 16a–h). Caspase-1 and gasdermin D are required for pyroptosis, but also for the release of IL-18, which is upstream of the perforin–caspase-7 defence pathway; thus, caspase-1 and gasdermin D are required for liver defence (Extended Data Fig. 16c). Consistently, caspase-7 was not required in other infectious models in which pyroptosis clears bacteria *in vivo* (Extended Data Fig. 16i–m). Therefore, in niches in which pyroptosis dominates as the regulated cell death defence, caspase-7 is not required. Conversely, when apoptosis is dominant with evasion of caspase-1—as seen during *L. monocytogenes* infection<sup>26,27</sup>—caspase-1 is not required for the perforin–caspase-7 defence pathway (Extended Data Fig. 16n).

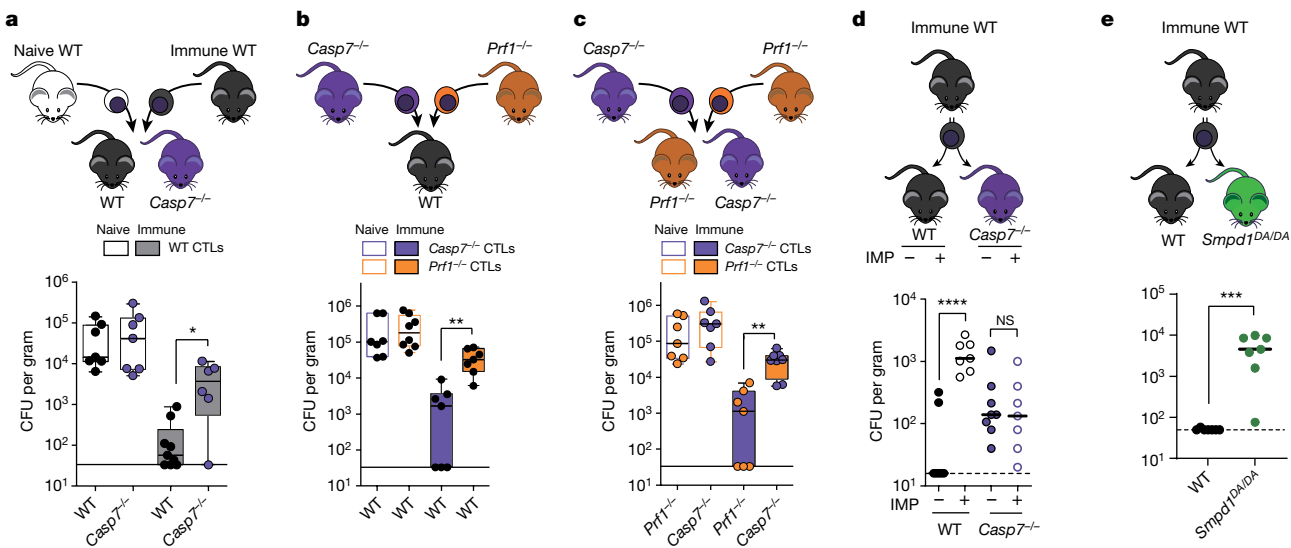


**Fig. 5 | Clearance of *L. monocytogenes* after CTL perforin attack requires cleavage of caspase-7 and ASM.** **a–c**, CTL donor mice were treated with PBS (naive) or vaccinated with *ΔactA*. *monocytogenes* (immune). Recipient mice were infected with *L. monocytogenes* and transferred with CTLs at 0 dpi, and the liver burdens were determined at 3 dpi. A timeline for the adoptive transfer experiments is shown in Extended Data Fig. 12d. **d**, Recipient mice were injected intraperitoneally with IMP or PBS (day -1 to infection, then daily). **e**, Recipient mice were infected with *L. monocytogenes* and transferred with immune CTLs at 0 dpi, and the liver burdens were determined at 3 dpi. All data

are pooled from two experiments. Mouse numbers: **a**, naive WT  $n = 7$ , immune WT  $n = 9$ , naive Casp7<sup>-/-</sup>  $n = 7$ , immune Casp7<sup>-/-</sup>  $n = 6$ ; **b**, WT mice with Casp7<sup>-/-</sup> CTLs  $n = 7$  each, naive Prf1<sup>-/-</sup> CTLs  $n = 8$ , immune Prf1<sup>-/-</sup> CTLs  $n = 7$ ; **c**, naive recipients  $n = 7$  each, immune recipients Prf1<sup>-/-</sup>  $n = 8$ , Casp7<sup>-/-</sup>  $n = 7$ ; **d**, WT  $n = 7$ , WT IMP  $n = 7$ , Casp7<sup>-/-</sup>  $n = 8$ , Casp7<sup>-/-</sup> IMP  $n = 7$ ; **e**, WT  $n = 7$ , Smpd1<sup>DA/DA</sup>  $n = 7$ . \* $P < 0.05$ , \*\* $P < 0.01$ , \*\*\* $P < 0.001$ , \*\*\*\* $P < 0.0001$ ; NS, not significant (two-sided Mann–Whitney *U*-test in **a**, **e**; one-way ANOVA in **b**–**d**). Bars indicate median values. Box plots show median and 25th–75th percentiles; whiskers are minimum and maximum values. Exact *P* values in Source Data.

## Phylogeny of caspase-7 and pores

Finally, we examined the phylogenetic conservation of Casp7, Prf1 and Gsdmd. Casp7 and Prf1 were present even within Chondrichthyes (sharks). However, Gsdmd first arises in marsupials and is absent in more-primitive organisms (Extended Data Fig. 16o). Therefore, caspase-7 and perforin arose long before gasdermin D. We speculate that the original evolved function of caspase-7 was to counteract perforin pores, and that a secondary function to counteract gasdermin D pores appeared later in evolution. If this is the case, it could explain why we observed stronger phenotypes in bacterial clearance during perforin-mediated immune defence.

## Discussion

Here we show that the unique function of caspase-7 is to activate ASM and thereby drive plasma membrane repair (see schematic in Extended Data Fig. 17). Our results indicate that ASM has two modes of action: basal activity and caspase-7-potentiated activity. Total loss of ASM causes Niemann–Pick disease, a lysosomal storage disease<sup>10</sup>. That Casp7<sup>-/-</sup> and Smpd1<sup>DA/DA</sup> mice are healthy provides evidence that caspase-7 cleavage is dispensable for basal ASM activity. The basal activity of pro-ASM-generated ceramide will rapidly repair a few pores in the plasma membrane without the need for caspase-7. Similarly, basal ESCRT-III-dependent exocytosis can repair gasdermin D or MLKL pore opening<sup>33,34</sup>; however, caspases are not known to enhance ESCRT-III function. Notably, the combined activity of the many basal membrane repair pathways, including basal ASM, ESCRT-III, constriction and patching<sup>10</sup>, do not compensate for the loss of caspase-7-enhanced membrane repair in our models. When caspase-7 cleaves ASM, this boosts the activity of ASM, which results in copious production of ceramide that repairs numerous membrane pores. Therefore, caspase-7 improves on the normal membrane repair capacity.

Gasdermin D and perforin pores will allow a massive influx of calcium, causing lysosomal exocytosis that will deliver pro-ASM to the

cell surface to repair the membrane. However, caspase-1, or NK cell or CTL attack, might generate numerous gasdermin or perforin pores that exceeds the basal membrane repair capacity. We propose a model in which activated caspase-7 passes through gasdermin D or perforin pores to encounter ASM. This is an elegant solution to enable caspase signalling to reach across the membrane to activate extracellular ASM. This caspase-7–ASM pathway provides one regulatory mechanism to slow down pore-mediated lysis. This should be in parallel to other regulatory mechanisms; for example, caspase-1 self-inactivation by cleavage between its CARD and protease domains<sup>35</sup>, and caspase-3 inhibition by XIAPs<sup>36</sup>.

Why membrane repair is required to facilitate the successful extrusion of IECs is a question that requires further attention. Opening the gasdermin D pore probably triggers IEC extrusion, but the open pore would also cause the loss of cytosolic molecules required to complete the extrusion process. For example, ATP is essential for normal actomyosin contraction in extruding IECs<sup>8</sup>. In the absence of repair, IECs might become depleted of ATP or other critical constituents before the extrusion process is completed. This incomplete extrusion could be detrimental to neighbouring cells, which could explain the abnormal clustering of extruding cells that we observe during *S. Typhimurium* infection in Casp7<sup>-/-</sup> and Smpd1<sup>DA/DA</sup> mice. The precise identity of the cytosolic extrusion effectors that are compromised under caspase-7 and ASM deficiency remains unknown.

Why membrane repair is essential to enable the clearance of intracellular bacteria after NK-cell- or CTL-mediated perforin attack is another unresolved point. There is evidence that multiple CTL attacks are required in vivo in other infectious models<sup>37</sup>, which would generate many perforin pores. These should be problematic for completing apoptosis because rapid swelling and membrane rupture might occur faster than caspase-3 can act<sup>38,39</sup>. Apoptosis requires time and intact cellular energetics. We speculate that caspase-7 permits the cell the time needed to complete apoptosis after perforin-mediated attack. We propose that completion of the apoptotic process is required to clear *C. violaceum* and *L. monocytogenes*, and that perforin-driven lysis

is not sufficient. However, why lysis would not be sufficient to clear the bacteria is not immediately apparent. Indeed, pyroptosis drives lysis in vivo to trap bacteria in pore-induced intracellular traps that lead to neutrophil efferocytosis, thereby killing bacteria;<sup>40</sup> this mechanism is likely to clear *C. violaceum* in the spleen. Which aspect of apoptosis leads to bacterial clearance from hepatocytes is a question that requires further investigation.

Overall, our results suggest that caspase-7 is not simply a weak back-up for caspase-3 during apoptosis. Instead, caspase-7 is a facilitator of cell death pathways that is independently essential during regulated cell death. Notably, in our IEC extrusion model caspase-7 acts downstream of the pyroptotic caspase-1, but in the NK cell and CTL model, caspase-7 acts downstream of granzyme B and probably in concert with the apoptotic caspase-3. We therefore propose to change the designation of caspase-7 from an apoptotic executioner to a general cell death facilitator that is useful for both inflammatory and apoptotic pathways when a cell needs to maintain an intact membrane for a certain period of time.

## Online content

Any methods, additional references, Nature Research reporting summaries, source data, extended data, supplementary information, acknowledgements, peer review information; details of author contributions and competing interests; and statements of data and code availability are available at <https://doi.org/10.1038/s41586-022-04825-8>.

1. Lamkanfi, M. et al. Targeted peptidecentric proteomics reveals caspase-7 as a substrate of the caspase-1 inflammasomes. *Mol. Cell. Proteomics* **7**, 2350–2363 (2008).
2. Sellin, M. E. et al. Epithelium-intrinsic NAIP/NLRC4 inflammasome drives infected enterocyte expulsion to restrict *Salmonella* replication in the intestinal mucosa. *Cell Host Microbe* **16**, 237–248 (2014).
3. Rauch, I. et al. NAIP-NLRC4 inflammasomes coordinate intestinal epithelial cell expulsion with eicosanoid and IL-18 release via activation of caspase-1 and -8. *Immunity* **46**, 649–659 (2017).
4. Kuida, K. et al. Decreased apoptosis in the brain and premature lethality in CPP32-deficient mice. *Nature* **384**, 368–372 (1996).
5. Lakhani, S. A. et al. Caspases 3 and 7: key mediators of mitochondrial events of apoptosis. *Science* **311**, 847–851 (2006).
6. Wu, C. et al. BioGPS: an extensible and customizable portal for querying and organizing gene annotation resources. *Genome Biol.* **10**, R130 (2009).
7. Reikvam, D. H. et al. Depletion of murine intestinal microbiota: effects on gut mucosa and epithelial gene expression. *PLoS One* **6**, e17996 (2011).
8. Marchiando, A. M. et al. The epithelial barrier is maintained by in vivo tight junction expansion during pathologic intestinal epithelial shedding. *Gastroenterology* **140**, 1208–1218 (2011).
9. Nozaki, K., Li, L. & Miao, E. A. Innate sensors trigger regulated cell death to combat intracellular infection. *Annu. Rev. Immunol.* **40**, 469–498 (2022).
10. Andrews, N. W., Almeida, P. E. & Corrotte, M. Damage control: cellular mechanisms of plasma membrane repair. *Trends Cell Biol.* **24**, 734–742 (2014).
11. Edelmann, B. et al. Caspase-8 and caspase-7 sequentially mediate proteolytic activation of acid sphingomyelinase in TNF-R1 receptosomes. *EMBO J.* **30**, 379–394 (2011).
12. Ferlinz, K. et al. Functional characterization of the N-glycosylation sites of human acid sphingomyelinase by site-directed mutagenesis. *Eur. J. Biochem.* **243**, 511–517 (1997).
13. Andrews, N. W., Corrotte, M. & Castro-Gomes, T. Above the fray: surface remodeling by secreted lysosomal enzymes leads to endocytosis-mediated plasma membrane repair. *Semin. Cell Dev. Biol.* **45**, 10–17 (2015).
14. Llacuna, L., Mari, M., Garcia-Ruiz, C., Fernandez-Checa, J. C. & Morales, A. Critical role of acidic sphingomyelinase in murine hepatic ischemia-reperfusion injury. *Hepatology* **44**, 561–572 (2006).
15. Müller, A. J. et al. The *S. Typhimurium* effector SopE induces caspase-1 activation in stromal cells to initiate gut inflammation. *Cell Host Microbe* **6**, 125–136 (2009).
16. Quan, L. T. et al. Proteolytic activation of the cell death protease Yama/CPP32 by granzyme B. *Proc. Natl Acad. Sci. USA* **93**, 1972–1976 (1996).
17. Darmon, A. J., Nicholson, D. W. & Bleackley, R. C. Activation of the apoptotic protease CPP32 by cytotoxic T-cell-derived granzyme B. *Nature* **377**, 446–448 (1995).
18. Chinnaiyan, A. M. et al. Cytotoxic T-cell-derived granzyme B activates the apoptotic protease ICE-LAP3. *Curr. Biol.* **6**, 897–899 (1996).
19. Gu, Y. et al. Processing and activation of CMH-1 by granzyme B. *J. Biol. Chem.* **271**, 10816–10820 (1996).
20. Orth, K., Chinnaiyan, A. M., Garg, M., Froelich, C. J. & Dixit, V. M. The CED-3/ICE-like protease Mch2 is activated during apoptosis and cleaves the death substrate lamin A. *J. Biol. Chem.* **271**, 16443–16446 (1996).
21. Jorgensen, I., Rayamajhi, M. & Miao, E. A. Programmed cell death as a defence against infection. *Nat. Rev. Immunol.* **17**, 151–164 (2017).
22. Batista, J. H. & da Silva Neto, J. F. *Chromobacterium violaceum* pathogenicity: updates and insights from genome sequencing of novel *Chromobacterium* species. *Front. Microbiol.* **8**, 2213 (2017).
23. Maltez, V. I. et al. Inflammasomes coordinate pyroptosis and natural killer cell cytotoxicity to clear infection by a ubiquitous environmental bacterium. *Immunity* **43**, 987–997 (2015).
24. Rongvaux, A. et al. Apoptotic caspases prevent the induction of type I interferons by mitochondrial DNA. *Cell* **159**, 1563–1577 (2014).
25. McArthur, K. et al. BAK/BAX macropores facilitate mitochondrial herniation and mtDNA efflux during apoptosis. *Science* **359**, eaao6047 (2018).
26. Sauer, J. D. et al. *Listeria monocytogenes* engineered to activate the NlrC4 inflammasome are severely attenuated and are poor inducers of protective immunity. *Proc. Natl Acad. Sci. USA* **108**, 12419–12424 (2011).
27. Warren, S. E. et al. Generation of a *Listeria* vaccine strain by enhanced caspase-1 activation. *Eur. J. Immunol.* **41**, 1934–1940 (2011).
28. Clark, S. E., Schmidt, R. L., McDermott, D. S. & Lenz, L. L. A *Batf3/Nlrp3/IL-18* axis promotes natural killer cell IL-10 production during *Listeria monocytogenes* infection. *Cell Rep.* **23**, 2582–2594 (2018).
29. Kägi, D., Ledermann, B., Bürki, K., Hengartner, H. & Zinkernagel, R. M. CD8+ T cell-mediated protection against an intracellular bacterium by perforin-dependent cytotoxicity. *Eur. J. Immunol.* **24**, 3068–3072 (1994).
30. Harty, J. T., Lenz, L. L. & Bevan, M. J. Primary and secondary immune responses to *Listeria monocytogenes*. *Curr. Opin. Immunol.* **8**, 526–530 (1996).
31. Hsu, K. M., Pratt, J. R., Akers, W. J., Achilefu, S. I. & Yokoyama, W. M. Murine cytomegalovirus displays selective infection of cells within hours after systemic administration. *J. Gen. Virol.* **90**, 33–43 (2009).
32. Kägi, D. et al. Cytotoxicity mediated by T cells and natural killer cells is greatly impaired in perforin-deficient mice. *Nature* **369**, 31–37 (1994).
33. Rühl, S. et al. ESCRT-dependent membrane repair negatively regulates pyroptosis downstream of GSDMD activation. *Science* **362**, 956–960 (2018).
34. Gong, Y. N. et al. ESCRT-III acts downstream of MLKL to regulate necrototic cell death and its consequences. *Cell* **169**, 286–300 (2017).
35. Boucher, D. et al. Caspase-1 self-cleavage is an intrinsic mechanism to terminate inflammasome activity. *J. Exp. Med.* **215**, 827–840 (2018).
36. Jost, P. J. et al. XIAP discriminates between type I and type II FAS-induced apoptosis. *Nature* **460**, 1035–1039 (2009).
37. Halle, S. et al. In vivo killing capacity of cytotoxic T cells is limited and involves dynamic interactions and T cell cooperativity. *Immunity* **44**, 233–245 (2016).
38. Keefe, D. et al. Perforin triggers a plasma membrane-repair response that facilitates CTL induction of apoptosis. *Immunity* **23**, 249–262 (2005).
39. Thiery, J. et al. Perforin activates clathrin- and dynamin-dependent endocytosis, which is required for plasma membrane repair and delivery of granzyme B for granzyme-mediated apoptosis. *Blood* **115**, 1582–1593 (2010).
40. Jorgensen, I., Zhang, Y., Krantz, B. A. & Miao, E. A. Pyroptosis triggers pore-induced intracellular traps (PITs) that capture bacteria and lead to their clearance by efferocytosis. *J. Exp. Med.* **213**, 2113–2128 (2016).

**Publisher's note** Springer Nature remains neutral with regard to jurisdictional claims in published maps and institutional affiliations.

© The Author(s), under exclusive licence to Springer Nature Limited 2022

# Article

## Methods

### Mice

Mice were housed in a specific-pathogen-free facility: wild-type C57BL/6 (The Jackson Laboratory), *Casp7<sup>-/-</sup>* (Jackson 006237), *Casp3<sup>-/-</sup>* (Jackson 006233; note these mice are born at sub-Mendelian ratios from heterozygous × heterozygous or heterozygous × homozygous breeding, with the latter often failing to breed; weaned *Casp3<sup>-/-</sup>* mice appear normal and healthy by visual inspection), *Gsdmd<sup>-/-</sup>* (ref. <sup>3</sup>), *Nlrc4<sup>-/-</sup>* (ref. <sup>41</sup>), *Casp1<sup>-/-</sup>*–*Casp11<sup>129mt/129mt</sup>* referred to as *Casp1<sup>-/-</sup>*–*Casp11<sup>-/-</sup>* (ref. <sup>42</sup>), *Casp6<sup>-/-</sup>* (Jackson 006236)<sup>43</sup> and *Prf1<sup>-/-</sup>* (Jackson 002407)<sup>32</sup> mice were used. *Smpd1<sup>D249A/D249A</sup>* mice (this paper; referred to as *Smpd1<sup>DA/DA</sup>*) were generated by the Duke Cancer Institute, breed normally and are healthy by visual inspection to at least five months of age at the time of publication. Animal protocols were approved by the Institutional Animal Care and Use Committee (IACUC) at the University of North Carolina at Chapel Hill or by the IACUC at Duke University and met guidelines of the US National Institutes of Health (NIH) for the humane care of animals. All strains were maintained on 12–12 light cycles, at 22.2 ± 1.1 °C, and under the humidity set point of 45%. All strains were maintained on the C57BL/6 background. For all mouse infections, 8–12-week-old mice were infected with the designated CFU or plaque-forming units (PFU). *C. violaceum*, *S. Typhimurium*, *Burkholderia thailandensis* and MCMV were delivered in PBS by intraperitoneal (IP) injection; *L. monocytogenes* and *L. monocytogenes ΔactA* mutant were delivered in PBS by intravenous (IV) injection; LCMV was delivered in Dulbecco's modified Eagle's medium (DMEM) by IP injection. For bacterial and viral enumeration, organs were bead-homogenized and serially diluted on brain heart infusion (BHI) agar plates (*C. violaceum*, *L. monocytogenes* and *L. monocytogenes ΔactA* mutant), Luria-Bertani (LB) agar plates (*S. Typhimurium* and *B. thailandensis*) or for plaque or 50% tissue culture infectious dose (TCID<sub>50</sub>) assays (LCMV and MCMV). Both male and female mice were used in equivalent numbers in groups unless otherwise stated. Mice were allocated to groups for experiments in a non-biased manner. Blinding of mice was not performed except for histological scoring of pathology. The target sample size was six mice per group, based on power analysis and historical trends in data variance; however, smaller or larger group sizes were used sometimes owing to mouse availability.

### Strains and growth conditions

Bacterial strains used in this work: *S. enterica* serovar Typhimurium on the 14028s background with or without *fLgB*::Tn10 were used for competitive index, comparing kanamycin vector control (pWSK129) to FliC<sup>ON</sup> (pEM087)<sup>44</sup>; *B. thailandensis* (strain previously passaged through a *Casp1<sup>-/-</sup>*–*Casp11<sup>-/-</sup>* mouse), *C. violaceum* (ATCC 12472), *L. monocytogenes* (10403s derivative, native *inlAB* replaced with mouse-specific *inlAmB*, PMC 2869327) and *L. monocytogenes ΔactA* mutant (a gift from the laboratory of D. Portnoy) were also used. We refer in the text to the *L. monocytogenes* strain with the mouse-specific *inlAmB* as wild-type *L. monocytogenes*. *C. violaceum*, *L. monocytogenes* and *L. monocytogenes ΔactA* mutant were grown in BHI. *S. Typhimurium* and *B. thailandensis* were grown in LB medium. All bacterial strains were grown overnight at 37 °C and back-diluted (1:40) for 2 h for all experiments.

Viral stocks of LCMV were generated from infected BHK-21 monolayers (laboratory of J.K.W.). Viral stocks of MCMV (Smith strain, ATCC VR-1399) were grown in 3T12 cells (ATCC), passaged in weanling BALB/c mice, collected from the salivary glands and quantified in viral plaque assays<sup>45</sup> (generated in the laboratory of M.G.B.).

### Tissue culture cell lines

L-WRN cells were purchased directly from ATCC, which is considered a reputable vendor; they were further authenticated by their phenotype of supporting organoid growth, a property that other cell lines cannot accomplish. HeLa cells were purchased from Duke University Cell Culture Facility, and were authenticated by short tandem repeat

(STR) analysis performed by this facility. Hepa1-6 and YAC-1 were purchased directly from ATCC, which is considered a reputable source. Hepa1-6 cells were partially authenticated by visual morphology. YAC-1 cells were partially authenticated by the phenotype of being attacked by NK cells. Cell lines were not further authenticated. Cell lines were tested for mycoplasma contamination. These cell lines are not included in the list of commonly misidentified cell lines by ICLAC.

### S. Typhimurium oral infection

For *S. Typhimurium* infection, streptomycin pretreatment was performed as previously described<sup>46</sup>. Mice were deprived of food and water for 4 h and treated orally with 20 mg kg<sup>-1</sup> streptomycin the day before infection. *S. Typhimurium* SL1344 was grown overnight at 37 °C and back-diluted (1:40) for 4 h in LB, then diluted in PBS before infection. Mice were deprived of food and water for 4 h, then *S. Typhimurium* was delivered by oral gavage on day 0 (5 × 10<sup>6</sup> CFU were used unless otherwise indicated). Water was provided thereafter, and food was provided 2 h later ad libitum. For ASM depletion, mice were injected IP with 10 mg kg<sup>-1</sup> IMP (Sigma I0899) or PBS control daily, starting from the day before infection. For *S. Typhimurium* enumeration, organs were collected, bead-homogenized and serially diluted on LB agar plates with streptomycin. Caeca were incubated in gentamycin–PBS (50 µg ml<sup>-1</sup>) for an hour, then washed three times and collected.

### Competitive index

For competitive indices with *S. Typhimurium*, bacteria were grown to stationary phase overnight in LB. Eight-to-ten-week-old mice were infected with 10<sup>5</sup> total CFU composed of vector control pWSK129 (kanamycin-resistant) mixed at a 1:1 ratio with FliC<sup>ON</sup> (ampicillin-resistant) *S. Typhimurium*. Bacteria were diluted in PBS and injected into mice by IP injection. Tissues were collected two days after infection and homogenized, and dilutions were plated onto LB plus antibiotics. Competitive index is expressed as log (FliC<sup>ON</sup> CFU/vector control CFU), thus a -2.0 competitive index reflects a ratio of 1 FliC<sup>ON</sup> to 100 vector control CFU.

### In vivo treatments

For NK cell depletion, mice were injected IP with 100 µg anti-NK1.1 (PK136, BioXcell, BE0036) or isotype control (C1.18.4, BioXCell, BE0085). Depletion of NK1.1-positive cells was confirmed by flow cytometry. For IL-18 therapies, mice were injected IP with 0.2 µg recombinant mouse IL-18 (rmIL-18; MBL) at the time of infection, and daily until collection as we previously described<sup>23</sup>. For ASM depletion, mice were injected IP with 10 mg per kg per mouse of IMP (Sigma) or PBS control beginning at day -1 before infection, then daily. For in vivo IFN $\gamma$  blockade, mice were injected IP with 500 µg per mouse of anti-mouse IFN $\gamma$  (XMG1.2, BioXcell, BE0055) or isotype (Rat IgG1, BioXcell BE0290) control beginning at day -1 before infection, then every other day.

### Enzyme-linked immunosorbent assay

Mice serum was collected and stored at -80 °C until use. IFN $\gamma$  levels in serum were determined by enzyme-linked immunosorbent assay (ELISA) (R&D Systems). For ELISA, 100 µl of capture antibody diluted in PBS was plated into a 96-well plate, covered with parafilm and left overnight at room temperature. After washing with wash buffer four times, blocking buffer was added (300 µl) and incubated for 1 h at room temperature. After washing four times, 100 µl of each sample and standard per well was added and reacted for 90 min at room temperature. After washing four times, 100 µl of detection antibody was added. After washing four times, 100 µl of streptavidin–horseradish peroxidase (HRP) was added and incubated for 20 min at room temperature. After development with 100 µl of substrate solution for 20 min, the reaction was stopped with 50 µl of 2N H<sub>2</sub>SO<sub>4</sub> and signal at 450 nm was detected using a Epoch Microplate Spectrophotometer (BioTek) running Gen 5 v.3.10 software.

### Induction of acute colitis by DSS

Mice were initially maintained on 2.5% w/v DSS (MP Biochemical 160110) ad libitum for 7 days, followed by 10 days of regular drinking water. Body weights were measured before the induction of colitis and daily thereafter until mice were euthanized. For histology, mice were treated with 2.5% w/v DSS ad libitum for 5 days and euthanized, then tissues were placed in 10% formalin for at least 24 h before embedding, cutting and H&E staining by the UNC Cell Services and Histology Core.

### Immunofluorescence and analysis

Caecum or organoid samples were fixed with 4% paraformaldehyde (PFA) in PBS overnight at 4 °C. Liver was perfused through the portal vein with 2% PFA in PBS and left to fix in 5 ml of 2% PFA overnight. After overnight incubation, samples were rinsed in PBS and replaced in 30% sucrose in PBS for two days, then embedded in OCT compound (Sakura Finetek 4583) and frozen on dry ice and cut into 5- to 8-μm sections.

Tissues were air-dried, washed in PBS and permeabilized with 1% Triton X-100 in PBS for 30 min, and blocked in 1% BSA PBS for 1 h at room temperature. Primary antibodies were incubated overnight. After washing in PBS for 10 min three times, secondary antibody reactions were performed for 2 h at room temperature, followed by another three washes in PBS. Finally, slides were mounted with DAPI (Fluoroshield, Sigma F6057).

Primary antibodies detecting cleaved caspase-7 (1:400, Cell Signaling 9491), cleaved caspase-3 (1:400, Cell Signaling 9661), EpCAM (1:1,000, BioLegend 118202, clone G8.8) and ceramide (both 1:200, ENZO Life Sciences ALX-804-196, clone MID15B4, and 1:200, Glycobio-tech MAB\_0014, clone S58-9, were used) in 1% BSA PBS were used. For hepatocyte or *Listeria* colocalization analyses, slides were then stained with CPS1 as a marker of hepatocytes<sup>47</sup> or a polyclonal anti-*Listeria* antibody (Abcam 68592, 1:10) for 1 h. Phalloidin (1:1,000, Invitrogen, A12379, A34055, A22287) was used to stain F-actin. Alexa-conjugated antibodies (anti-rabbit; Cell Signaling 4412, 4414; anti-rat, Abcam ab175475; anti-mouse, Invitrogen A10037) were used as secondary antibodies (1:1,000). Anti-PARP1 antibody (D214, STJ90100, St John's Laboratory; 1:400) was also used.

For TUNEL staining, tissues were instead fixed in 4% PFA and permeabilized with 0.2% Triton, with 0.2% Triton remaining in all further staining steps. Slides were stained overnight for cleaved caspase-7 as above. Tissues were then stained for TUNEL signal with the Roche *in situ* cell death detection kit TMR red (Sigma 12156792910). Mounting medium contained DAPI.

All images were taken on a Zeiss 880 machine with a Plan-Neofluar 40×/1.3 objective operated by ZEN Black Edition v.14.0 software, or Olympus BX61 machine. The images shown in Extended Data Fig. 9 are composed of multiple merged 20× images in the zones of cleaved caspase-3 or caspase-7 staining, which were overlaid above a 10× image that occupies the upper left quadrant of the image (where there is primarily DAPI staining).

Anti-CPS1-HRP antibody was obtained from Abcam (198969, 1:300) and is an intracellular marker (thus requires fixation and permeabilization before antibody use). HRP-conjugated antibodies can be used with tyramide signal amplification techniques to generate a fluorescent signal detectable by flow cytometry and immunofluorescence. AlexaFluor 488 signal was generated using the Thermo Fisher Scientific kit T20922, and cells or tissues were incubated with the solution for 10 min before stopping the reaction and washing. Endogenous peroxidase signal was blocked with 0.3% hydrogen peroxide for 60 min before incubation with anti-CPS1 antibody.

### Isolation, culture and treatment of IECs

Jejunal-ileal crypts were isolated from 10-to-15-week-old wild-type mice as previously described<sup>48</sup>. After euthanasia, the intestine was removed and cut open, then washed three times, followed by

2.5 mM EDTA chelation for 30 min at 4 °C and mechanical dissociation. The isolated crypts were pelleted and washed three times in 2% sorbitol PBS with low-speed centrifugation (400 rpm, 3 min) at 4 °C and resuspended in 1% FCS/DMEM. After being filtered through 70-μm strainers, crypts were pelleted and embedded in Matrigel (BD Biosciences 356321) and incubated for 20 min at 37 °C. After gels were solidified, warmed 50% L-WRN conditioned media from L-WRN cells (ATCC 3276) based on Advanced DMEM/F12 (Gibco 12634010) were added<sup>49</sup>. These conditioned media were supplemented with 20 ng ml<sup>-1</sup> mouse EGF (Peprotech 315-09). The medium was changed every two days until the following use of cultured organoids. For organoid imaging experiments, day-2 organoids from various genotypes were grown for a further 24–48 h in Advanced DMEM/F12 containing 1× glutamax, 1× penicillin-streptomycin, 2.5 mM N-acetylcysteine (Sigma A9165), 500 ng ml<sup>-1</sup> mouse Rspo1 (R&D Systems 3474-RS-050), 20 ng ml<sup>-1</sup> mouse EGF and 100 ng ml<sup>-1</sup> mouse Noggin (R&D Systems 6997-NG-025) to allow differentiation.

For organoid stimulation, 3 μg ml<sup>-1</sup> FlaTox<sup>50</sup>, 20 ng ml<sup>-1</sup> TNF (Peprotech 315-01A), 5 μg ml<sup>-1</sup> CHX (Sigma C4859) and 50 μM IMP (Sigma I7379) were used. For organoid imaging experiments, PI (100 μg ml<sup>-1</sup>, Invitrogen P3566) was loaded before 1 h of imaging. Calcein-AM (2 μM, Invitrogen C3100) was loaded before 30 min of experiments as per the manufacturer's protocol. For ceramide introduction, 1 mM of C-16 ceramide (Cayman Chemical 10681) stock solution was prepared in N,N-dimethylformamide (Sigma D4551). C-16 ceramide (final concentration; 500 nM) or control vehicle was added to the cell culture medium before 2 h 30 min of imaging.

### Time-lapse imaging of organoids

Time-lapse imaging of the organoids were performed on MetaMorph v.7.10 software on a VivaView Incubator Fluorescence Microscope (Olympus) with an X-Cite eXacte as the illumination source. Differential interference contrast (DIC) images as well as fluorescent images (PI and calcein) were acquired through a UPLSAPO 20× objective (0.75 NA) onto an Orca R2 cooled CCD camera (Hamamatsu). After 30 min to 1 h of adaption, single-plane imaging was performed for 1.5–6 h at 120–320-s intervals just after treatment with FlaTox or TNF + CHX. ImageJ v.1.4.3.67 software (NIH) was used to measure the mean intensity of each organoid in a hyperstack image for PI and calcein intensity analysis.

### Liver cell enrichment

Livers were extracted and perfused with collagenase type I (1 mg ml<sup>-1</sup> in RPMI) by portal vein injection until visible blanching of all lobes was observed. Liver lobes were then finely cut into small pieces using a razor blade and incubated for 10 min at 37 °C with CO<sub>2</sub>. They were then mashed through a cell strainer (Falcon, 70 μm) into a 50-ml conical and washed with around 40 ml of plain RPMI. Cells were spun in a tabletop centrifuge (Eppendorf, model 5810R) at 50g for 5 min at 4 °C. The supernatant was discarded, the pellet resuspended in 15 ml of RPMI and spun for an additional two times at 50g for 5 min at 4 °C. The cell pellets, now consisting of more than 96% hepatocytes (as previously reported<sup>51</sup> and validated by flow cytometry) were resuspended once in PBS and spun again as before. Cells were resuspended in RBC lysis buffer, incubated for 5 min at room temperature (around 22 °C), spun at 1,500 rpm in a small tabletop centrifuge (Eppendorf model 5810R) and the pellet resuspended in RPMI or 1× PBS depending on usage. For splenocyte isolation, spleens were mashed through a cell strainer (Falcon, 70 μm) into a 50-ml conical and washed with 15 ml of plain RPMI. Cells were spun at 1,000g for 5 min, once in RPMI, and once in PBS. They were then RBC-lysis-treated, spun and the pellet resuspended in RPMI or 1× PBS.

### Adoptive transfer of NK cells

Splenocytes were collected from naive mice as described above. Cells were seeded into 10-cm non-tissue-culture-treated dishes with

# Article

RPMI + 10% fetal bovine serum (FBS) + non-essential amino acids (NEAA) + penicillin-streptomycin + 15 ng ml<sup>-1</sup> IL-2. Four days later, the supernatant was removed and spun at 1,000 rpm for 5 min to remove dead cells. The supernatant was returned to the dish along with 2 ml of new medium with an additional 10 ng ml<sup>-1</sup> of IL-2. Six days after initial plating, the cells were counted and used for transfer.

## Adoptive transfer with enumeration of bacterial count

For experiments using bacterial counts from *L. monocytogenes*, donor mice were vaccinated with  $1 \times 10^6$  of the *DactA* *L. monocytogenes* mutant strain or mock-injected with PBS as described previously<sup>52</sup>. NK cells were depleted (see 'In vivo treatments' above) in all donor mice on day 5 after challenge to remove potential confounding NK contributions. Splenocytes were collected from naive or immunized mice as described above. Recipient mice were then adoptively transferred by IV injection with  $5 \times 10^7$  bulk splenocytes. One-hour after adoptive transfer, recipient mice were IV injected with  $5 \times 10^4$  CFU of *L. monocytogenes*. Livers and spleens were collected three days later, homogenized and dilutions plated on BHI. Plates were incubated at 37 °C and bacterial counts were enumerated 16–24 h later.

## Adoptive transfer with flow and immunofluorescence analysis

For experiments examining the expression of cleaved caspase-7 (Extended Data Fig. 12) in *L. monocytogenes* infections, donor mice were vaccinated, NK cells were depleted and splenocytes were collected as in the adoptive transfer experiments described above ('In vivo treatments' and 'Adoptive transfer of NK cells'). Recipient mice were IV injected with  $5 \times 10^4$  *L. monocytogenes* two days before adoptive transfer. Recipient mice were then transferred with  $8 \times 10^7$  bulk splenocytes by IV injection. Mice were euthanized 24 h after adoptive transfer. One lobe of the liver was prepared for immunofluorescence, and hepatocytes were isolated from the remaining liver lobes for flow cytometry (see 'Liver cell enrichment' above and 'Flow cytometry' below).

## Flow cytometry

Surface and intracellular staining was performed directly ex vivo. Cells were Fc-blocked with anti-CD16/CD32 (1:100) and surface stained with anti-CD45.2-PercPCy5.5 (104, Biolegend 109828; 1:400), anti-NK1.1-FITC (PK136, Biolegend 108706; 1:400) and anti-CD8a (Biolegend 109807; 1:400). Cells were fixed in 2% PFA either overnight at 4 °C or for 20 min on ice before permeabilizing with 10× Fix/Perm Buffer (Biolegend 421002) on ice. Cells were incubated with cleaved caspase-7 antibody (Cell Signaling 9491, 1:500, 45 min) followed by APC-conjugated secondary anti-rabbit antibody (Cell Signaling, 4414s, 1:1,000, 45 min). After five washes, cells were stained with anti-CPS1-HRP antibody (Abcam 198969, 1:300, detailed description below, 45 min), and samples were analysed on a FacsCalibur machine courtesy of the laboratory of J.K.W. Flow cytometry data were collected using BD CellQuest Pro v.5.2.1 software and analysed using FlowJo v.10.3 software.

## Quantification of viral titre

LCMV viral titre in the liver was quantified by plaque assay on Vero cell monolayers<sup>53</sup>. MCMV viral titre in the liver was quantified by TCID<sub>50</sub> assay on 10.1 mouse embryonic fibroblasts (MEFs). MEFs were seeded at 5,000 cells per well into 96-well plates and allowed to adhere for 24 h. Serial dilutions of liver homogenate were then added and cultured for six days before determining cytopathic effects. Titre was determined using the Reed-Muench method.

## In vitro co-culture assays

NK cells were expanded ex vivo as follows: splenocytes were collected from naive mice as described above. Cells were seeded into 10 cm non-TC-treated dishes with RPMI + 10% FBS + NEAA + penicillin-streptomycin + 15 ng ml<sup>-1</sup> IL-2. Four days later, the supernatant was removed and spun at 1,000 rpm for 5 min to remove dead cells.

The supernatant was returned to the dish along with 2 ml of new medium with an additional 10 ng ml IL-2<sup>-1</sup>. Six days after initial plating, the cells were counted and used for transfer. Hepa1-6 cells (mouse hepatocyte cell line; ATCC CRL-1830) were maintained in DMEM with 10% FBS. Cells were seeded at  $5 \times 10^4$  cells per well of a treated 96-well plate and allowed to adhere overnight. The following day (approximately 24 h later), they were infected at a multiplicity of infection (MOI) of 0.5 with *L. monocytogenes* for 1 h before washing and replacing with medium containing gentamicin (50 µg µl<sup>-1</sup>). The next morning (approximately 16 h later), the cells were washed to remove gentamicin from all wells, and co-cultured with NK cells at an effector:target (E:T) ratio of 5:1 with or without gentamicin added to the medium. Bacterial counts and caspase-3 or -7 activation were analysed 5 h after co-culture.

YAC-1 cells (non-adherent mouse lymphoblast cell line; ATCC TIB-160) are inherently targeted by NK cells and often used for NK killing assays. YAC-1 cells were maintained in RPMI with 10% FBS. They were also seeded at  $5 \times 10^4$  cells per well of a treated 96-well plate. They were infected for 1 h at a MOI of 10 with either *C. violaceum* or *L. monocytogenes* before washing and replacing with medium containing gentamicin (50 µg µl<sup>-1</sup>) for 1 h. YAC-1 cells were then washed, co-cultured with NK cells and analysed for bacterial counts and caspase-3 or -7 activation as with the Hepa1-6 cells.

## In vitro granzyme B

For each experiment, Hepa1-6 cells were lifted and  $1 \times 10^6$  cells per replicate for each treatment condition were lysed in 50 µl of 1% Triton X-100. Purified recombinant mouse granzyme B (PeproTech 140-03) was then added at the indicated amounts (0.2, 0.4 or 0.8 µg) and incubated with the lysates for 1 h at room temperature. A small volume (10 µl) was removed at the end of the hour to validate the cleavage of caspase-3 and -7 by western blot. Then 50 µl containing  $1 \times 10^6$  *L. monocytogenes* was added and incubated at room temperature. Small volumes of lysate were dilution-plated over 16 h to quantify possible effects on bacterial viability in the presence of granzyme B, active caspase-3 and active caspase-7.

## Western blots

The amount of total protein from organoid lysates was normalized in a BCA kit (Pierce); proteins were resolved on NuPage precast 4%–12% Bis-Tris gels (Invitrogen) and were transferred to polyvinylidene difluoride membranes. After blocking in 2% BSA/TBST for 40 min at room temperature, primary antibody was added and incubated overnight at 4 °C. Caspase-3 cleavage was analysed using a cleavage-specific antibody (1:500, Cell Signaling 9661). Caspase-7 cleavage was analysed using a cleavage-specific antibody (1:500, Cell Signaling 9491). Caspase-1 cleavage (1:200, Santa Cruz sc-514 clone M-20), caspase-8 cleavage (1:500, Cell Signaling 8592) and caspase-9 cleavage (1:400, Cell Signaling 9504) were detected using those antibodies. Gasdermin D was analysed using an antibody detecting both the full-length and the cleaved form (1:500, Abcam ab209845). GAPDH (1:1,000, Cell Signaling 97166) was detected as an internal control. After washing in TBST three times, secondary antibody was added and incubated for 2 h at room temperature. Secondary HRP-conjugated anti-rabbit antibody was purchased from Cell Signaling (1:2,000, Cell Signaling 7074). After three washes in TBST, signals were developed with ECL substrates (Thermo Fisher Scientific) and analysed.

For the detection and validation of ASM, ASM-knockout HeLa cell lines were generated with CRISPR-Cas9 technology at the Duke Functional Genomics Core. Two-guide RNA targeting was used (target sites; 5'-GAACCCAATGTGGCTCGCGT-3' and 5'-ACAA TGGATTGGCACAGGGC-3').

For the detection of ASM in IECs, organoids were isolated from ECM and washed three times in PBS with low-speed centrifugation (850 rpm × 1 min). After dead cell removal, each organoid from various genotypes was separated equally into two parts, then treated with or

without FlaTox and both incubated for 20 min at 37 °C. After incubation, organoids were collected and lysed, then ASM was detected (1:1,000, Invitrogen PA-5 72432).

ASM was deglycosylated with PNGase F (New England BioLabs P0704) per the manufacturer's protocol. In brief, lysates were denatured at 100 °C for 10 min in glycoprotein denaturing buffer, chilled and centrifuged quickly, then incubated with PNGase F in GlycoBuffer at 37 °C for 1 h. After the reaction, ASM was detected by western blot.

### Histological scoring

For *S. typhimurium* infection, histology was assessed using a modified scheme adapted from a previous study<sup>46</sup>. Slides were blind scored (0 to 3) for each of four criteria: epithelial hyperplasia and damage; immune infiltrate into the mucosa and lamina propria; goblet cell loss; and submucosal oedema. The average score of four criteria was then calculated. For DSS experiments, slides were blind scored based on a previous report<sup>54</sup>. Three major criteria (0 to 3)—crypt hyperplasia, inflammatory cell infiltration and muscle thickening—and two minor criteria (0 to 1)—goblet cell depletion and crypt abscess—were used. These criteria were added together.

### Immunofluorescence quantification in the intestine

For the quantification of cleaved-caspase-7-positive cells, cleaved-caspase-3-positive cells, and EpCAM-positive cells, 60 to 90 fields with 40× Lenz in each mouse sample were randomly examined and the number of DAPI<sup>+</sup> caspase-7<sup>+</sup> cells, DAPI<sup>+</sup> caspase-3<sup>+</sup> cells or DAPI<sup>+</sup>EpCAM<sup>+</sup> cells was counted.

### Immunofluorescence quantification in the liver

For both *C. violaceum* and *L. monocytogenes* infections, inflammatory foci or lesions were easily identifiable by the visualization of abundant immune cell nuclei in the DAPI channel, and random lesions were selected for multi-channel pictures. These were split into single-channel images and regions of interest (ROI) were drawn around the foci using the DAPI channel as a guide (in ImageJ); thus, we were blinded for cleaved caspase-7 intensity. The ROI was copied to the single-channel image with cleaved caspase-7 and the integrated density was measured. Background integrated density (defined as the signal in an area outside the lesions) was subtracted for the reported values.

To analyse *C. violaceum*-infected liver images, multiple 10× pictures were stitched together owing to the large size of the lesions, and two lesions per mouse were quantified for cleaved caspase-7 signal (Extended Data Fig. 9a,b, quantification in Extended Data Fig. 9c). The number of CPS1 and cleaved caspase-7 double-positive cells was determined in Extended Data Fig. 9d. This was done by drawing a ROI encompassing 45 cells on the CPS1 single-channel image and copying it to the cleaved caspase-7 single-channel image. The percentage of double-positive cells was calculated for one region per IL-18-treated mouse, with six regions scored and plotted as the mean with standard deviation. Cleaved-caspase-7-positive cells were scored as CPS1-positive or -negative.

Cleaved caspase-7 signal was quantified from five lesions per mouse for *L. monocytogenes*-infected livers at 20× magnification (Extended Data Fig. 12d, quantification in Extended Data Fig. 12g). The percentage of cleaved-caspase-7-positive signal colocalizing with *L. monocytogenes* staining was determined in Extended Data Fig. 12i from three lesions per mouse.

### Organoid quantification

For the organoid rupture counting experiment, 10–20 organoids after FlaTox treatment were tracked for 2–3 h in each live-imaging experiment to determine their rupture behaviour. When the organoid architecture collapsed and the inner content of the organoid composed mostly of extruded IECs increased and ruptured into the exterior of the organoid, this was determined to be one ruptured organoid. All of the ruptured

organoids were counted and calculated as one rupture ratio shown as one indicative dot in the graphs, and were then pooled and combined.

For examining the extrusion starting time, the time when a total of four cells in one organoid started extrusion was recorded as the extrusion initiation time of that organoid to exclude the non-specific (homeostatic) epithelial extrusion.

For examining the PI or calcein intensity of the organoid, single-plane imaging was performed for 1.5–6 h at 180–480-s intervals just after FlaTox or TNF + CHX treatment. ImageJ software (NIH) was used to measure the mean intensity of each organoid in a hyperstack image and the average of the mean intensity in each time point was calculated.

### Expression data analysis

For BioGPS expression data, the indicated genes were used as queries (<http://www.biogps.org>)<sup>6</sup>. Mouse data from the dataset: GeneAtlas MOE430, gcrma were selected<sup>7</sup>, and the raw data were downloaded from the download tab. Selected organ data were graphed. The mean and s.e.m. are shown from two data points. For purified IEC expression data, the dataset GDS3921 (ACCN) was searched in the GEO Dataset Brower at NCBI (<https://www.ncbi.nlm.nih.gov/gds>). This dataset consists of previously published expression data from purified IECs<sup>7</sup>. Indicated genes were used as search terms for this dataset, and on the results page the graph image was selected to access the raw data page. Raw data from the value (count) chart were collated and plotted from the control mice that were not treated with antibiotics. Antibiotic-treated mouse data is not shown but results were equivalent. The mean with s.e.m. are shown from six data points.

### Statistics

Error bars represent the standard deviation of technical replicates and bars indicate median. Two-tailed unpaired *t*-test, two-tailed Mann–Whitney *U*-test, one-way ANOVA with Tukey's multiple comparison test and log-rank Mantel–Cox test were used for statistical analysis. *P* values of  $\leq 0.05$  were considered significant. Statistical analysis was performed using GraphPad Prism v.5 and v8 software and Microsoft Excel 2013.

### Reporting summary

Further information on research design is available in the Nature Research Reporting Summary linked to this paper.

### Data availability

All relevant data are included in the Article or its Supplementary Information files. More details are available from the corresponding author upon request. Source data are provided with this paper.

41. Mariathasan, S. et al. Differential activation of the inflammasome by caspase-1 adaptors ASC and Ipaf. *Nature* **430**, 213–218 (2004).
42. Kuida, K. et al. Altered cytokine export and apoptosis in mice deficient in interleukin-1 beta converting enzyme. *Science* **267**, 2000–2003 (1995).
43. Zheng, T. S., Hunot, S., Kuida, K. & Flavell, R. A. Caspase knockouts: matters of life and death. *Cell Death Differ.* **6**, 1043–1053 (1999).
44. Miao, E. A. et al. Caspase-1-induced pyroptosis is an innate immune effector mechanism against intracellular bacteria. *Nat. Immunol.* **11**, 1136–1142 (2010).
45. Wheat, R. L., Clark, P. Y. & Brown, M. G. Quantitative measurement of infectious murine cytomegalovirus genomes in real-time PCR. *J. Virol. Methods* **112**, 107–113 (2003).
46. Barthel, M. et al. Pretreatment of mice with streptomycin provides a *Salmonella enterica* serovar Typhimurium colitis model that allows analysis of both pathogen and host. *Infect. Immun.* **71**, 2839–2858 (2003).
47. Butler, S. L. et al. The antigen for Hep Par 1 antibody is the urea cycle enzyme carbamoyl phosphate synthetase 1. *Lab. Invest.* **88**, 78–88 (2008).
48. Sato, T. et al. Single Lgr5 stem cells build crypt-villus structures in vitro without a mesenchymal niche. *Nature* **459**, 262–265 (2009).
49. Miyoshi, H. & Stappenbeck, T. S. In vitro expansion and genetic modification of gastrointestinal stem cells in spheroid culture. *Nat. Protoc.* **8**, 2471–2482 (2013).
50. von Moltke, J. et al. Rapid induction of inflammatory lipid mediators by the inflammasome in vivo. *Nature* **490**, 107–111 (2012).
51. Gregory, S. H., Jiang, X. & Wing, E. J. Lymphokine-activated killer cells lyse *Listeria*-infected hepatocytes and produce elevated quantities of interferon-γ. *J. Infect. Dis.* **174**, 1073–1079 (1996).

# Article

52. Badovinac, V. P. & Harty, J. T. Adaptive immunity and enhanced CD8+ T cell response to *Listeria monocytogenes* in the absence of perforin and IFN- $\gamma$ . *J. Immunol.* **164**, 6444–6452 (2000).
53. Ahmed, R., Salmi, A., Butler, L. D., Chiller, J. M. & Oldstone, M. B. Selection of genetic variants of lymphocytic choriomeningitis virus in spleens of persistently infected mice. Role in suppression of cytotoxic T lymphocyte response and viral persistence. *J. Exp. Med.* **160**, 521–540 (1984).
54. Cooper, H. S., Murthy, S. N., Shah, R. S. & Sedergran, D. J. Clinicopathologic study of dextran sulfate sodium experimental murine colitis. *Lab. Invest.* **69**, 238–249 (1993).

**Acknowledgements** We thank R. Flavell, V. Dixit, R. Vance and M. Deshmukh for sharing mice directly or through The Jackson Laboratory. This work was supported by the following NIH grants: AI097518, AI133236, AI139304, AI119073, AI136920 (E.A.M.) AI097518-02S1 (V.I.M.), R56AI110682 and R01AI074862 (J.K.W.), R01AI050072 (M.G.B.) and P30CA016086 (UNC Flow Core). We also thank T. Abele, F. Lakhani, M. Artunduaga, M. DePrizio, S. Pereles, A. Vaidyanathan, R. Eplett, M. Mann, S. Reddecke and L. Scarpelli for mouse colony upkeep.

**Author contributions** K.N. led the IEC project, V.I.M. led the NK cell and CTL project, and K.N. led the ASM aspects of both projects. E.A.M. supervised. K.N. and E.A.M. discovered the IEC

extrusion defect and the ASM mechanism for the IEC and the NK cell and CTL models, and thereby unified the projects. V.I.M. and E.A.M. discovered the NK cell and CTL phenotypes. M.R. and E.A.M. initiated the project. In the IEC project, K.N. performed most of the experiments, with M.R. and A.L.T. performing some experiments. In the NK cell and CTL project, V.I.M. performed most of the experiments; K.N. performed ASM experiments; and J.E.M., C.A.L., C.K.H., L.L. and W.T.N. performed some experiments. H.N.L. and B.D.M. managed the mouse colony. N.J.M., M.G.B., J.K.W. and E.A.M. supervised the work. K.N., V.I.M. and E.A.M. wrote the paper. K.N. and E.A.M. oversaw the completion of the paper.

**Competing interests** C.A.L. is employed by AbbVie. This article is composed of the authors' work and ideas and does not reflect the ideas of AbbVie.

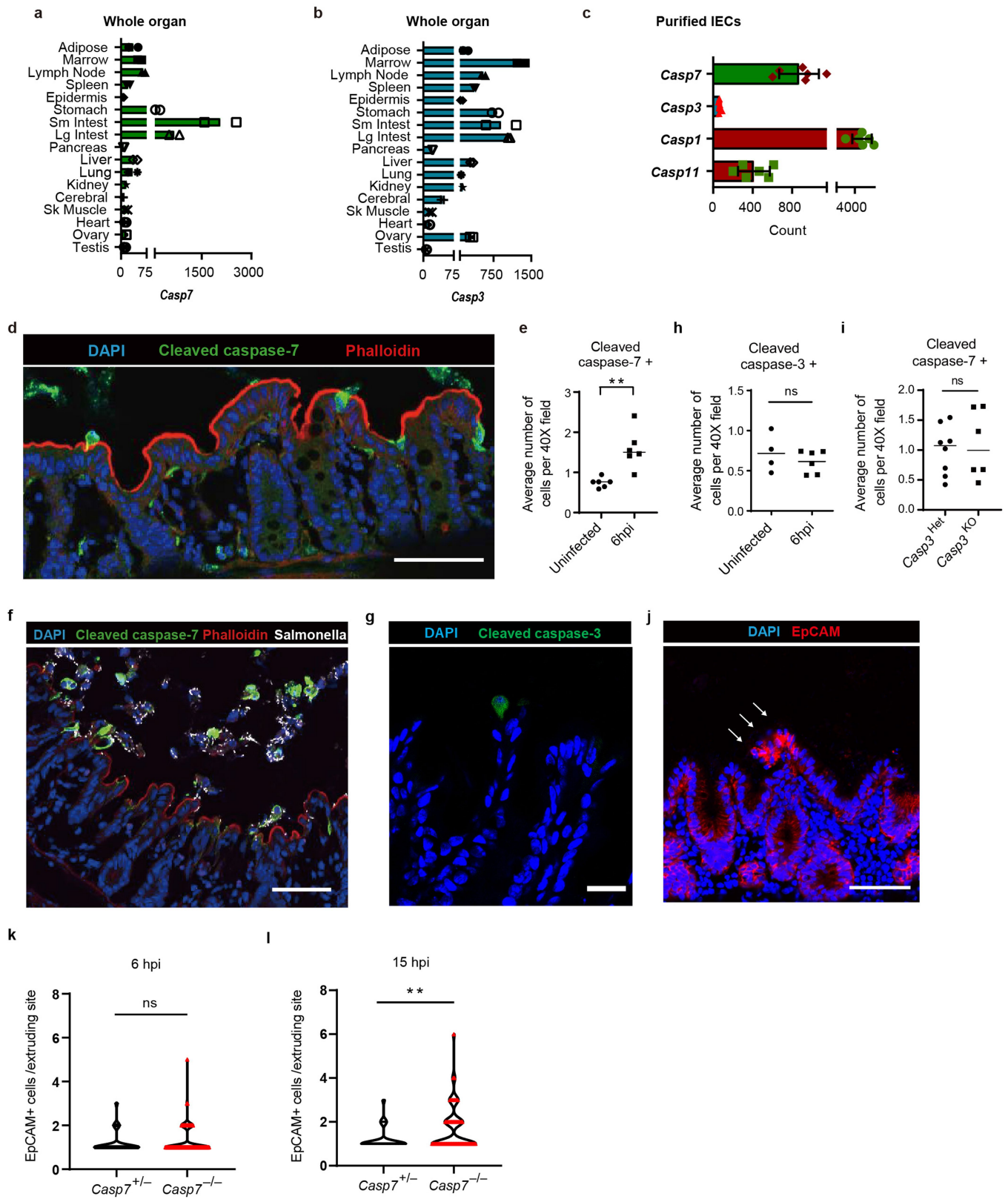
#### Additional information

**Supplementary information** The online version contains supplementary material available at <https://doi.org/10.1038/s41586-022-04825-8>.

**Correspondence and requests for materials** should be addressed to Edward A. Miao.

**Peer review information** *Nature* thanks Jonathan Kagan and the other, anonymous, reviewer(s) for their contribution to the peer review of this work. Peer reviewer reports are available.

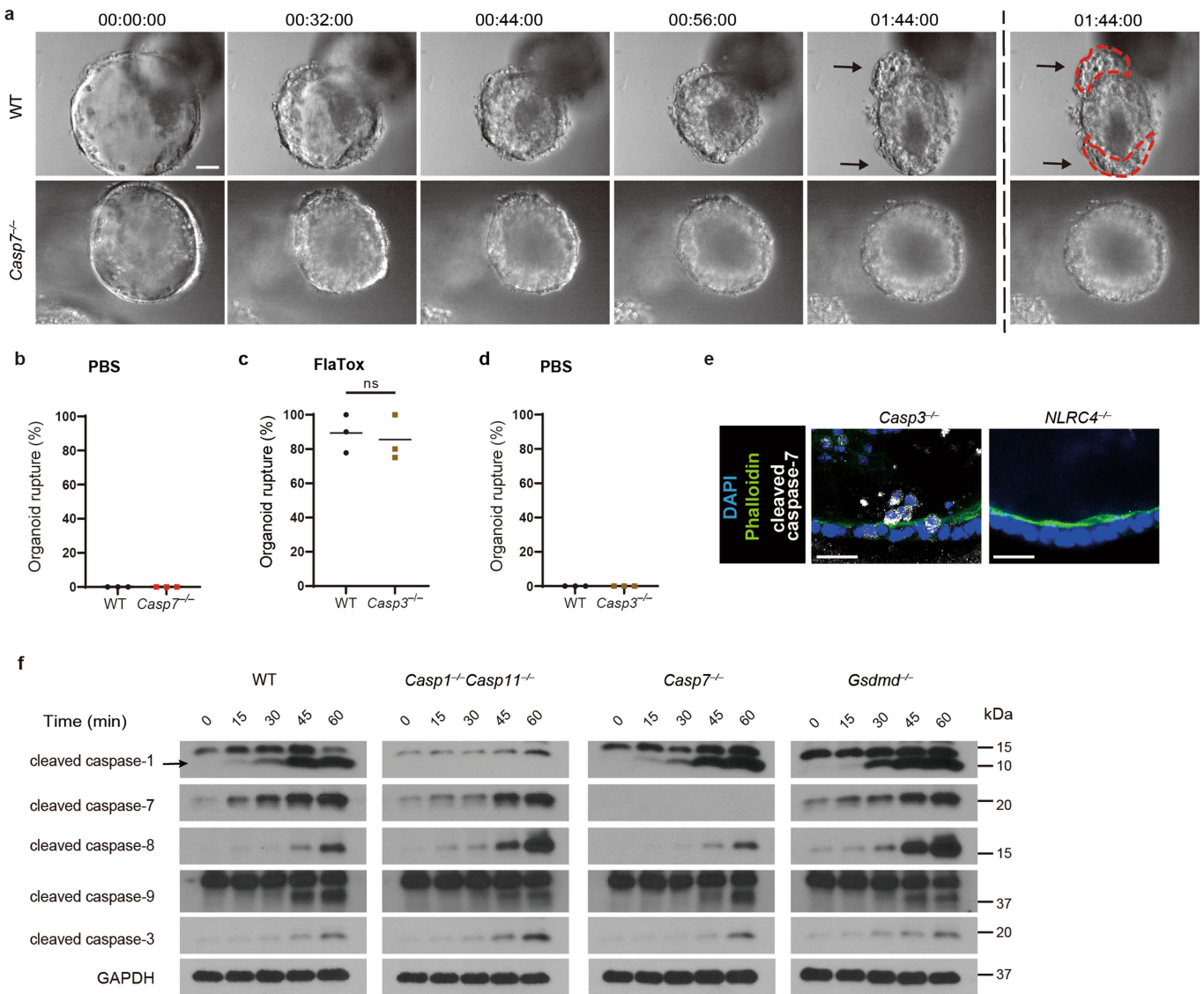
**Reprints and permissions information** is available at <http://www.nature.com/reprints>.



**Extended Data Fig. 1** | See next page for caption.

# Article

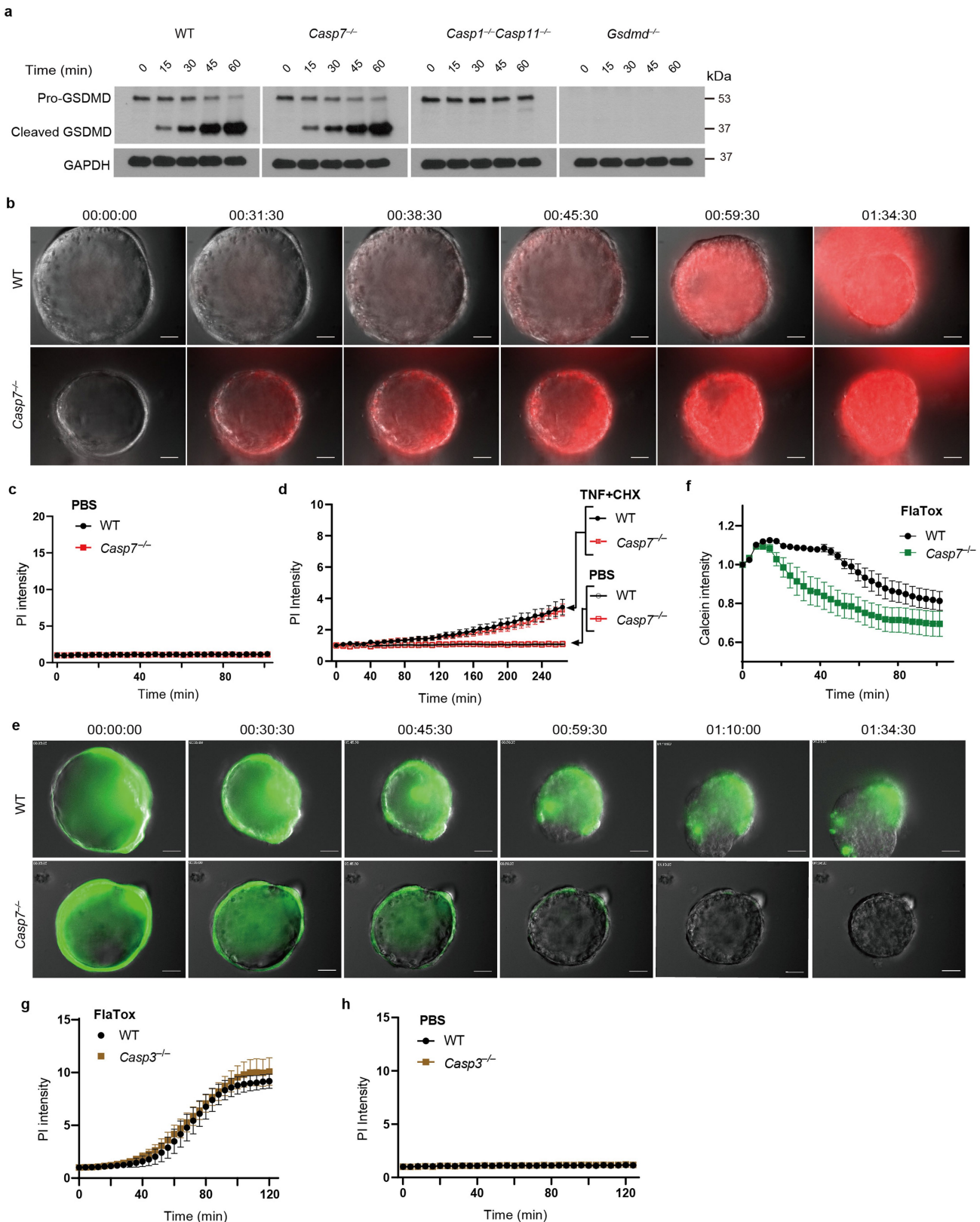
**Extended Data Fig. 1 | Caspase-7 is required for efficient IEC extrusion during *S. Typhimurium* infection.** **a-b**, Caspase-7 and caspase-3 mRNA levels in various tissues from  $n = 2$  samples were examined using BioGPS (biogps.org)<sup>6</sup>. **c**, Caspase-7, caspase-3, caspase-1 and caspase-11 expression levels in isolated IEC from  $n = 6$  samples were determined by from published transcriptome data<sup>7</sup>. **d-e**, Representative image (**d**) of cleaved caspase-7 staining of caecum from WT mice 6 h post-infection (hpi) with  $10^6$  *S. Typhimurium* and its quantification with uninfected control (uninfected mice ( $n = 6$ ) and infected mice ( $n = 6$ )). **(e)**. **f**, Cleaved caspase-7 staining of caecum from WT mice 12 hpi with  $10^6$  GFP-*S. Typhimurium*. **g-h**, Representative image (**g**) of cleaved caspase-3 staining of caecum from WT mice 6 hpi with  $10^6$  *S. Typhimurium* and its quantification with uninfected control (uninfected mice ( $n = 4$ ) and infected mice ( $n = 6$ )) (**h**). **i**, Quantitation in as in (**d**) for littermate-controlled *Casp3<sup>+/−</sup>* ( $n = 8$ ) and *Casp3<sup>−/−</sup>* mice ( $n = 6$ ). **j**, EpCAM staining of caecum from *Casp7<sup>−/−</sup>* mice 24 hpi with  $5 \times 10^6$  *S. Typhimurium* ( $\rightarrow$ , extrusion site with 18 clustered cells was one of the largest observed, related to Fig. 1a,b). **k-l**, quantitation of EpCAM+ cells per extruding site in caecum from littermate *Casp7<sup>+/−</sup>* and *Casp7<sup>−/−</sup>* mice 6 hpi (**k**) or 15 hpi (**l**) with  $5 \times 10^6$  *S. Typhimurium*; from the same experiment as the 24 hpi time point in Fig. 1b. Data are representative of 2 experiments (**e, h, i**), 3 experiments (**d, f, g**) or 1 experiment (**a-c, k, l**). Scale bar = 50  $\mu$ m. \* $P < 0.05$ , \*\* $P < 0.01$ , \*\*\* $P < 0.001$ , \*\*\*\* $P < 0.0001$  (Two-sided Mann–Whitney *U*-test). Data are shown as median  $\pm$  SEM. Exact  $p$  values in Source Data EDF1.



**Extended Data Fig. 2 | Caspase-7 facilitates IEC extrusion after FlaTox treatment.** **a**, Representative images of WT and *Casp7* $^{-/-}$  organoids after FlaTox treatment in 12 pooled experiments. **b**, Percentage of ruptured WT and *Casp7* $^{-/-}$  organoids after PBS treatment in pooled live imaging experiments. **c-d**, Percentage of ruptured WT and *Casp3* $^{-/-}$  organoids after FlaTox (**c**) or PBS (**d**) treatment in pooled experiments. **e**, Representative images of indicated

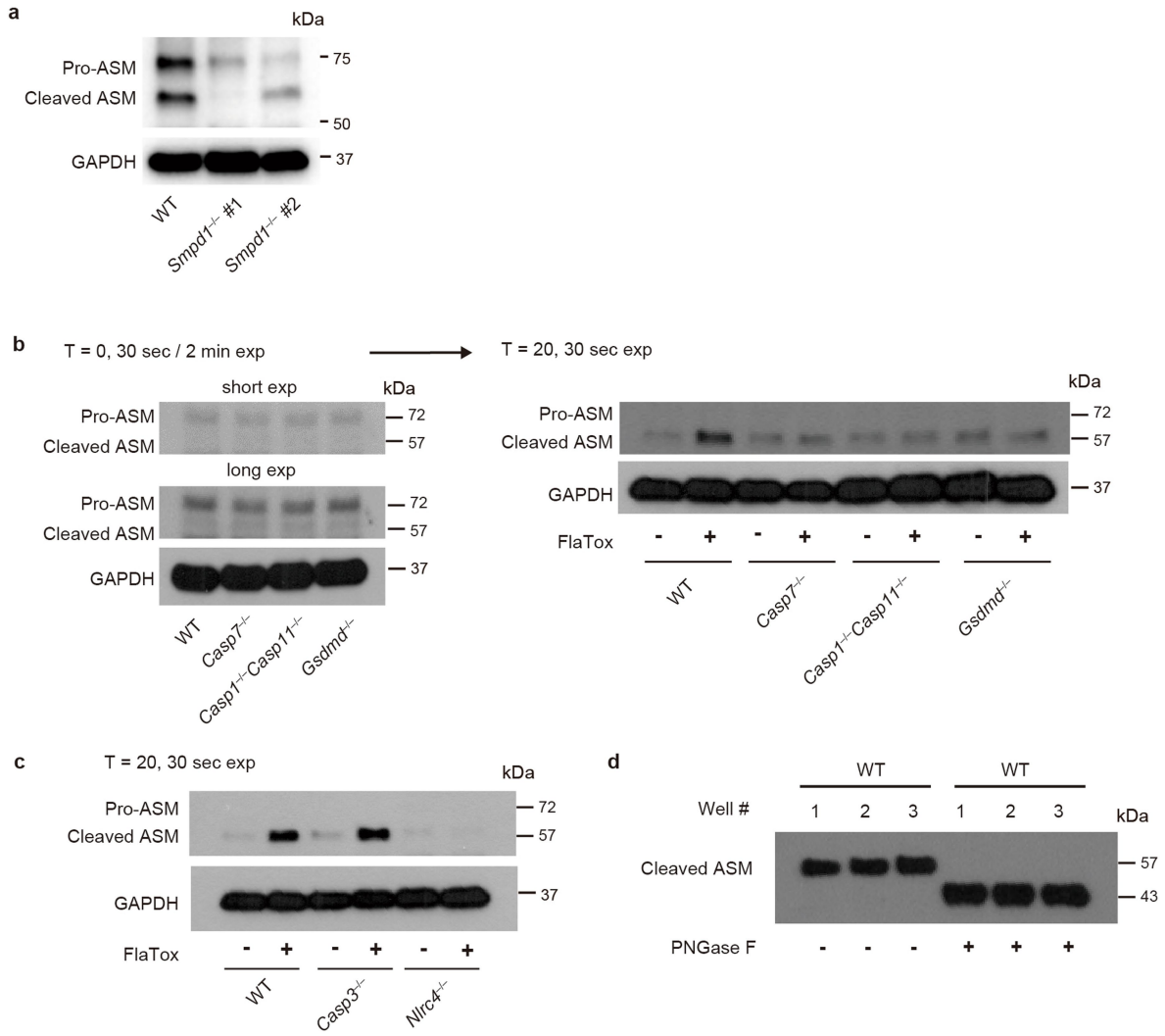
organoids 30 min after FlaTox treatment, stained with phalloidin and for cleaved caspase-7 (Related to Fig. 1d). **f**, Immunoblot of IEC organoids treated with FlaTox probed for the indicated caspases. Data are representative of 3 experiments (**e, f**) or pooled from 12 (**a**), or 3 (**b-d**) experiments. Scale bar = 20  $\mu$ m. \* $P < 0.05$ , \*\* $P < 0.01$ , \*\*\* $P < 0.001$ , \*\*\*\* $P < 0.0001$  (Two-sided unpaired *t*-test). Data are shown as mean  $\pm$  SEM. Exact p values available in Source Data EDF2.

# Article



**Extended Data Fig. 3 | Caspase-7 prolongs membrane integrity against gasdermin D pores.** **a**, Gasdermin D (GSDMD) cleavage in organoids treated with Flatox. **b**, Representative images in live-cell imaging showing PI intensity of WT and *Casp7*<sup>-/-</sup> organoids treated with Flatox. **c-d**, Quantitation of PI intensity in live-cell imaging of WT and *Casp7*<sup>-/-</sup> organoids treated with PBS (c) or TNF + CHX or PBS control (d). **e-f**, Representative images (e) and

quantitation (f) in live-cell imaging of calcein intensity of WT and *Casp7*<sup>-/-</sup> organoids treated with Flatox. **g-h**, Quantitation in live-cell imaging of PI intensity of WT and *Casp3*<sup>-/-</sup> organoids treated with Flatox (g) or PBS (h). Data are representative of 3 experiments. Scale bar = 50  $\mu$ m. \* $P$ <0.05, \*\* $P$ <0.01, \*\*\* $P$ <0.001, \*\*\*\* $P$ <0.0001 (Two-way ANOVA with Sidak's post-hoc test). Data shown as mean  $\pm$  SEM. Exact  $p$  values in Source Data EDF3.

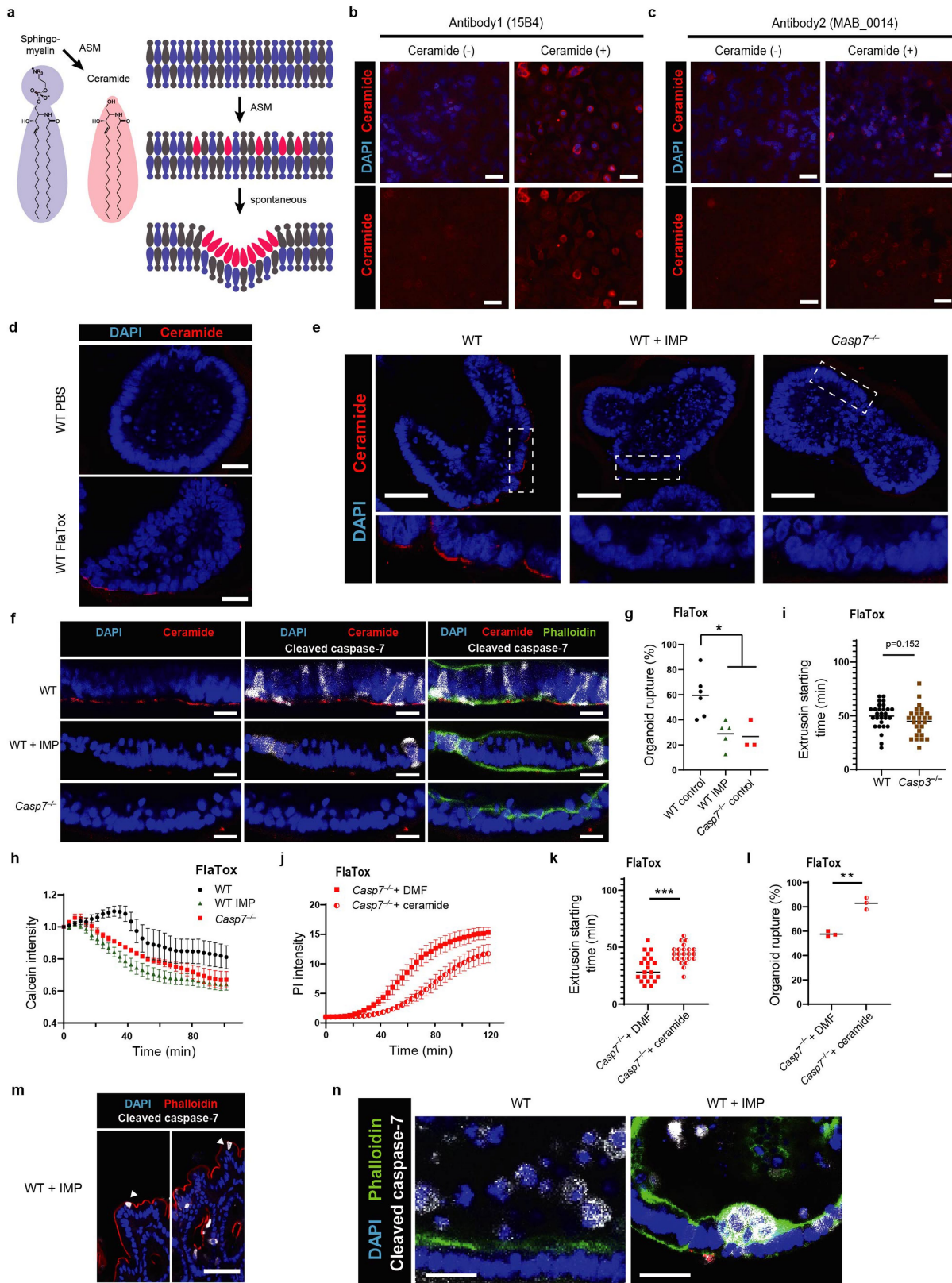


#### Extended Data Fig. 4 | ASM cleavage by caspase-7 requires gasdermin D.

**a**, Validation of ASM antibody performed by immunoblot of Crispr/CAS9 targeted HeLa cells. **b–d**, ASM cleavage of organoids that were removed of dead cells and stimulated 20 min with FlaTox. **(b)** organoid cells were split into 3 tubes, one for T = 0 without stimulation (left blots, shorter 30 s exposure and longer 2 min exposure) and two for 20 min PBS or FlaTox treatment (right blot,

shorter 30 s exposure). **(c)** ASM cleavage from WT, *Casp3*<sup>-/-</sup>, or *Nlrc4*<sup>-/-</sup> organoids. **(d)** WT organoid lysates treated with FlaTox in **(b)** was mock or treated with PNGase F to remove glycosylation; a band shift excludes the possibility that the 57-kDa band represents a deglycosylation event of pro-ASM. Data are representative of 3 experiments.

# Article

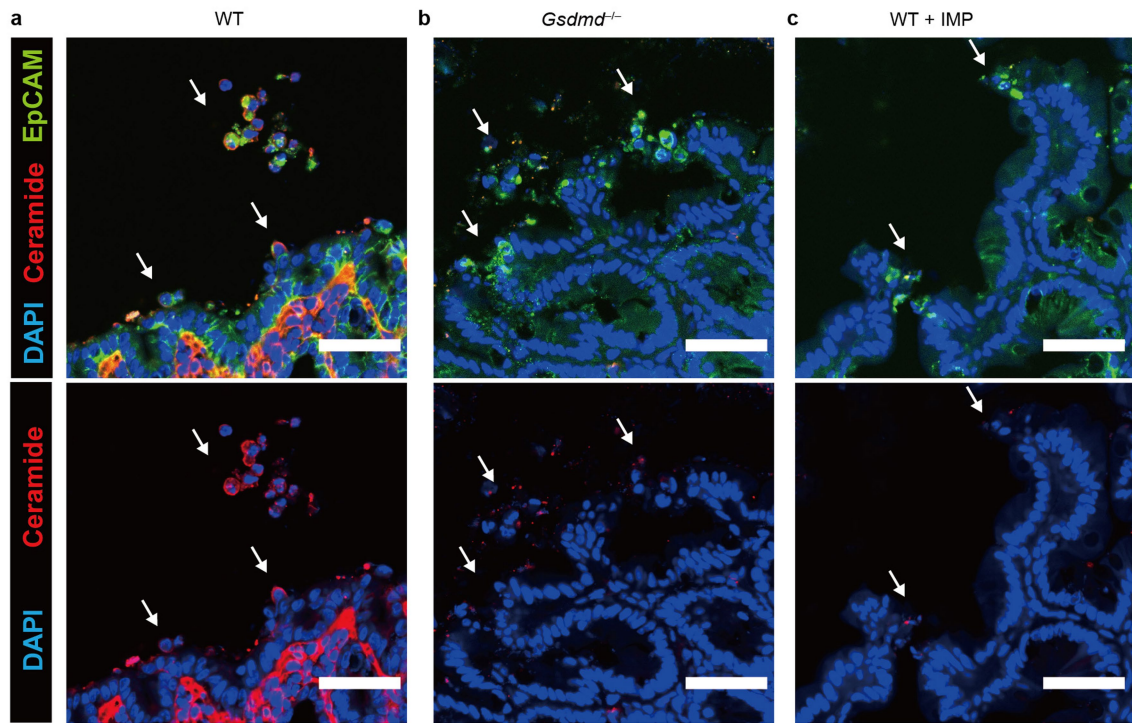


Extended Data Fig. 5 | See next page for caption.

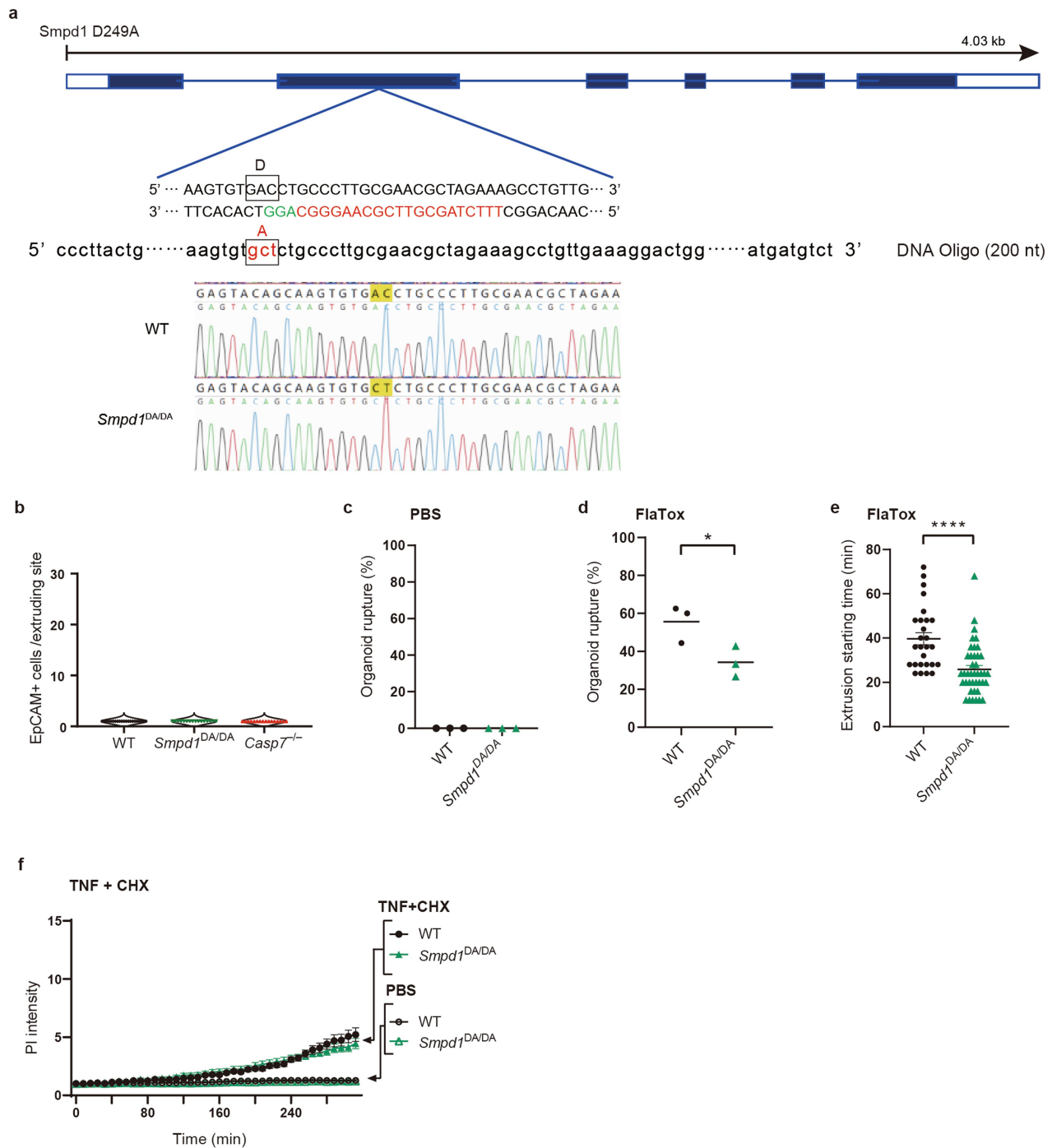
**Extended Data Fig. 5 | Caspase-7 activates ASM to generate ceramide.**

**a**, Established mechanism whereby sphingomyelin is cleaved by ASM to generate ceramide, a lipid that naturally invaginates membranes to drive membrane repair via endocytosis (adapted from (Andrews et al., 2014)<sup>10</sup>). **b-c**, Ceramide specificity of anti-ceramide antibodies was validated by treating HeLa cells with exogenous C-16 ceramide for 2.5 h followed by staining with the anti-ceramide antibodies 15B4 (**b**) or MAB\_0014 (**c**). **d**, Ceramide staining of WT organoids at 20 min post PBS or FlaTox. **e**, Ceramide staining of organoids at 20 min post FlaTox, with inset expanded images of the boxed areas. **f**, Ceramide and cleaved caspase-7 staining of indicated organoids at 20 min post FlaTox. **g-i**, Live imaging of indicated organoids after FlaTox treatment, quantitated for rupture percentage (**g**), calcein intensity (**h**), or extrusion starting time (**i**). **j-l**, Live imaging of indicated *Casp7<sup>-/-</sup>* + dimethylformamide (DMF) or vehicle or *Casp7<sup>-/-</sup>* + ceramide organoids after FlaTox treatment with quantitation of PI intensity (**j**), extrusion starting time

(**k**), or rupture percentage (**l**). **m**, Cleaved caspase-7 staining of caecal tissues from IMP-treated WT mice 24 hpi with  $5 \times 10^6$  S. Typhimurium, related to Fig. 2d (> indicates cleaved caspase-7+ cells that appear stuck in the monolayer and lack normal extrusion morphology). **n**, Cleaved caspase-7 staining of WT and WT+IMP organoids at 30 min post FlaTox. Data are representative of 2 experiments (**b, c**) or 3 experiments (**d-f, j, m-n**), or are pooled from 3 experiments (**h, l**). For (**g**), live Imaging of WT ( $n = 6$  datasets), WT+IMP ( $n = 5$  datasets), and *Casp7<sup>-/-</sup>* ( $n = 3$  datasets) organoids pooled from 7 experiments were analysed. For (**i**), WT ( $n = 28$ ) and *Casp3<sup>-/-</sup>* ( $n = 27$ ) organoids pooled from 3 experiments were analysed. For (**k**), *Casp7<sup>-/-</sup>* + DMF ( $n = 21$ ) and *Casp7<sup>-/-</sup>* + ceramide ( $n = 23$ ) organoids pooled from 3 experiments were analysed. Scale bar = 20  $\mu\text{m}$  (**b-d, f, n**), 50  $\mu\text{m}$  (**e, m**). \* $P < 0.05$ , \*\* $P < 0.01$ , \*\*\* $P < 0.001$ , \*\*\*\* $P < 0.0001$  (Two-sided unpaired *t*-test in (**g, i, k, l**), two-way ANOVA with Tukey's post-hoc test in (**h**) or with Sidak's post-hoc test in (**j**)). Data are shown as mean  $\pm$  SEM. Exact *p* values in Source Data EDF5.



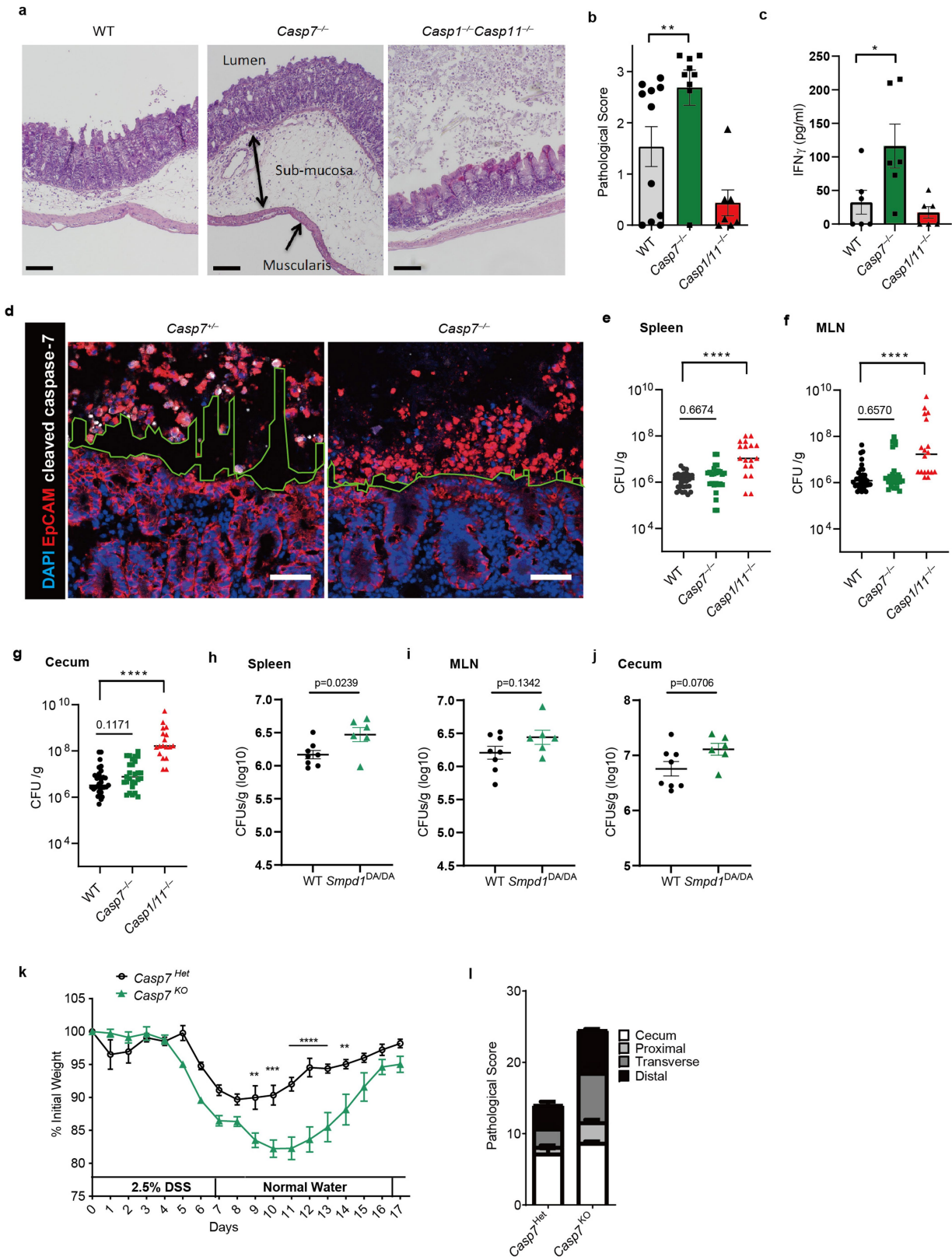
**Extended Data Fig. 6 | Ceramide production by caspase-7 requires gasdermin D pores.** a–c, Ceramide and EpCAM staining of caecum from WT (a), *Gsdmd*<sup>-/-</sup> (b), or WT+IMP (c) mice 24 hpi with  $5 \times 10^6$  S. Typhimurium ( $\rightarrow$ , extruding or extruded cells). Scale bar = 50  $\mu$ m. Data are representative of 3 experiments.



**Extended Data Fig. 7 | ASM cleavage is required for IEC extrusion.** **a**, Strategy to generate ASM D249A mutant mice by CRISPR–Cas9. Target sequence for guide RNA in exon 2 is shown in red. Repair oligo DNAs (200 nt) containing indicated mutation are also used for electroporation with Cas9. Successful mutation was confirmed by Sanger sequencing. **b**, Quantification of EpCAM+ cells per extruding site in non-infected WT, *Smpd1*<sup>DA/DA</sup>, and *Casp7*<sup>-/-</sup> caeca (n = 4 in each group). **c–f**, Live imaging of indicated IEC organoids, which were quantified for rupture percentage after PBS (**c**) or FlaTox (**d**) treatment,

extrusion starting time after FlaTox treatment (**e**), and PI Intensity after TNF+CHX or PBS treatment (**f**). Data are pooled from 2 (**b**) or 3 (**c–d**) experiments or are representative of 3 experiments (**f**). For (**e**), WT (n = 27) and *Smpd1*<sup>DA/DA</sup> (n = 41) organoids pooled from 3 experiments were analysed. \*P < 0.05, \*\*P < 0.01, \*\*\*P < 0.001, \*\*\*\*P < 0.0001 (Two-sided unpaired t-test in (**d**, **e**), two-way ANOVA with Sidak's post-hoc test in (**f**)). Data are shown as mean ± SEM. Exact p values in Source Data EDF7.

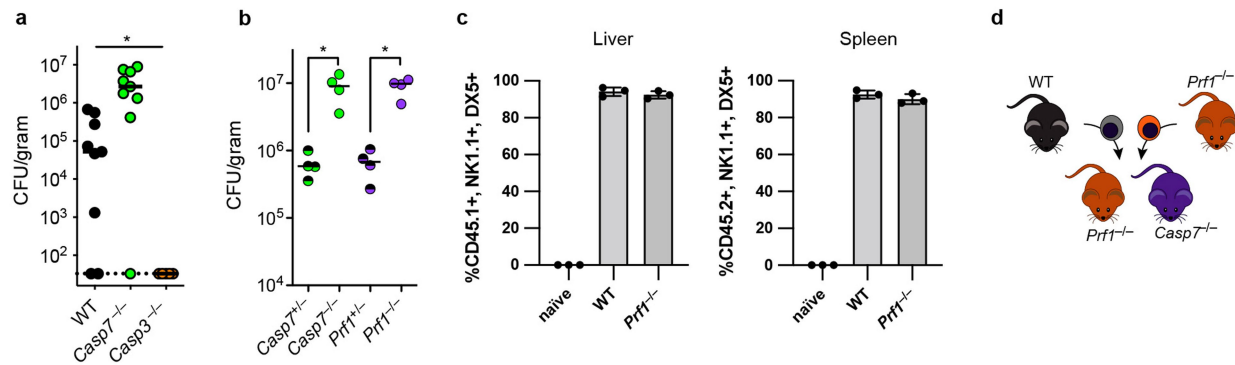
# Article



Extended Data Fig. 8 | See next page for caption.

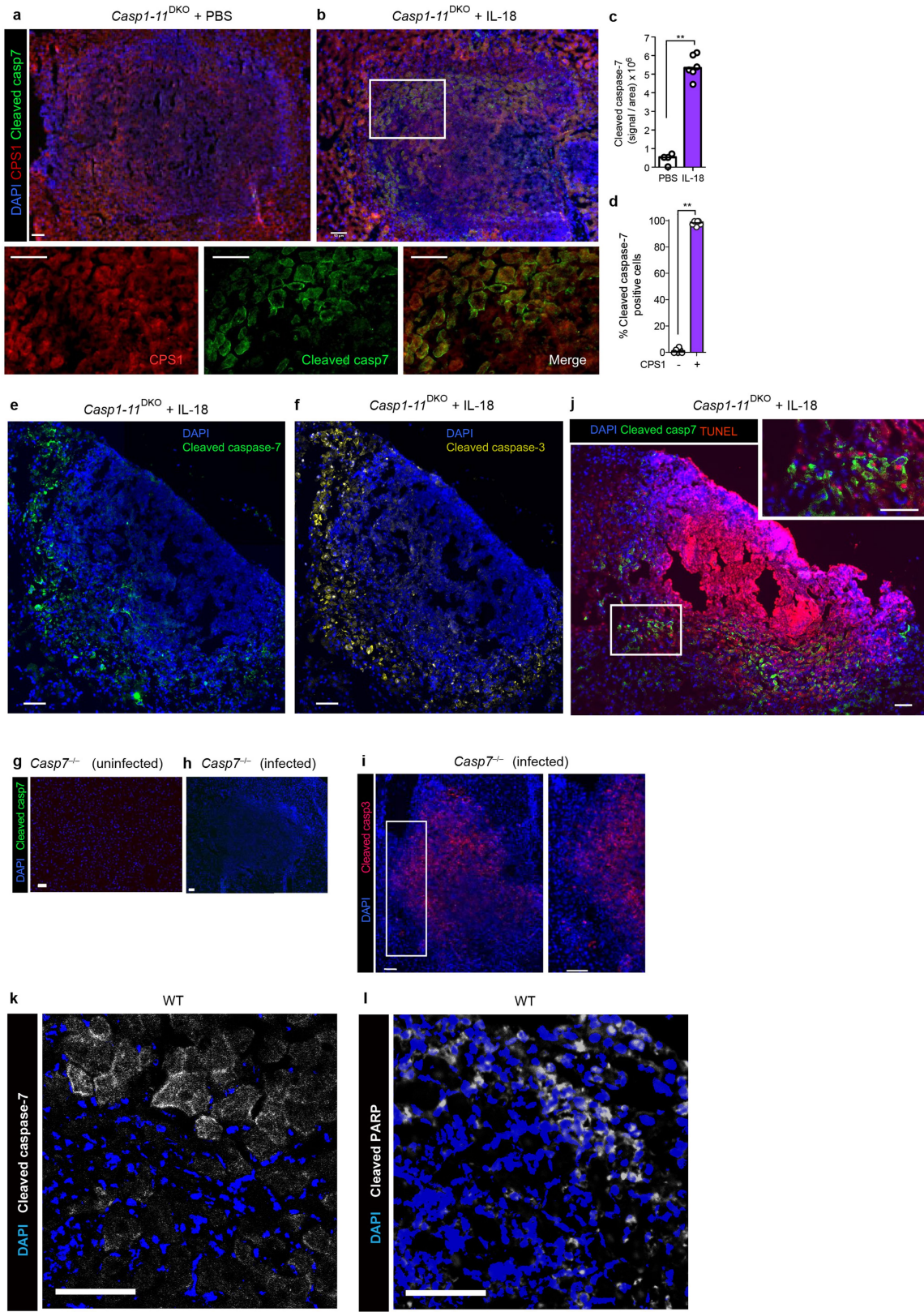
**Extended Data Fig. 8 | Caspase-7 ameliorates tissue pathology during *S. Typhimurium* infection or DSS colitis.** **a–c.** The indicated mice were infected with  $10^6$  *S. Typhimurium* for 2 days, then caeca were collected and stained with H&E. Shown are representative images (**a**) (Scale bar = 100  $\mu\text{m}$ ), pathological score (**b**) of WT ( $n=11$ ), *Casp7*<sup>-/-</sup> ( $n=9$ ), and *Casp1*<sup>-/-</sup>*Casp11*<sup>+/+</sup> ( $n=7$ ) mice, and serum IFN $\gamma$  (**c**) of WT, *Casp7*<sup>-/-</sup>, and *Casp1*<sup>-/-</sup>*Casp11*<sup>+/+</sup> mice ( $n=6$ ). **d.** EpCAM staining of caeca from littermate *Casp7*<sup>-/-</sup> and *Casp7*<sup>-/-</sup> mice 2 dpi with  $5 \times 10^6$  *S. Typhimurium*. Dotted lines indicate the space between the extruding IECs and epithelial layer. Scale bar = 50  $\mu\text{m}$ . **e–g.** CFU of WT ( $n=31$ ), *Casp7*<sup>-/-</sup> ( $n=27$ ), and *Casp1*<sup>-/-</sup>*Casp11*<sup>+/+</sup> ( $n=18$ ) mice 4 dpi with  $10^6$  *S. Typhimurium* in spleen (**e**), MLN (**f**), and gentamicin-treated caecum

(**g**). **h–j.** CFU of WT ( $n=8$ ) and *Smpd1*<sup>DA/DA</sup> ( $n=6$ ) mice 4 dpi with  $10^6$  *S. Typhimurium* in (**h**) spleen, (**i**) MLN, and (**j**) gentamicin-treated caecum. **k–l.** *Casp7*<sup>+/+</sup> and *Casp7*<sup>-/-</sup> mice treated with the indicated time course of DSS. Mouse weight (**k**) and pathology score (**l**) at day 5. Data are representative of 2 experiments with (**a**, **b**, **d**, **k**, **l**), or are pooled from 2 experiments (**c**), 3 experiments (**h–j**), or 5 experiments (**e–g**). \* $P < 0.05$ , \*\* $P < 0.01$ , \*\*\* $P < 0.001$ , \*\*\*\* $P < 0.0001$  (Two-sided Mann–Whitney *U*-test in (**b**), two-sided unpaired *t*-test in (**c**, **h–j**), one-way ANOVA with Dunnett’s post-hoc test in (**e–g**), two-way ANOVA with Sidak’s post-hoc test in (**k**)). Data are shown as mean  $\pm$  SEM. Exact *p* values in Source Data EDF8.



**Extended Data Fig. 9 | Caspase-7 and perforin phenocopy defence against *C. violaceum* infection.** **a–b**, Mice were infected IP with  $10^4$  *C. violaceum* and bacterial burdens in the liver were determined at 3 dpi for separately bred mice (**a**) or littermate-controlled mice (**b**). **c**, Ly5A<sup>+</sup> splenocytes were collected from wild-type mice and expanded ex vivo in IL-2 for the NK adoptive transfer experiments in Fig. 4d,e. Shown is the percentage of transferred cells that were

NK cells. **d**, NK cell adoptive transfer schematic for experiments in Fig. 4d,e. Data are pooled from 2 experiments in (**a**), representative of two experiments in (**b**), and representative of 3 experiments in (**c**). \* $P < 0.05$ , \*\* $P < 0.01$ , \*\*\* $P < 0.001$ , \*\*\*\* $P < 0.0001$  (One-way ANOVA (**a**) or two-sided Mann–Whitney *U*-test (**b**)). Bars indicate mean with standard deviation (**c**). Exact *p* and *n* values in Source Data EDF9.

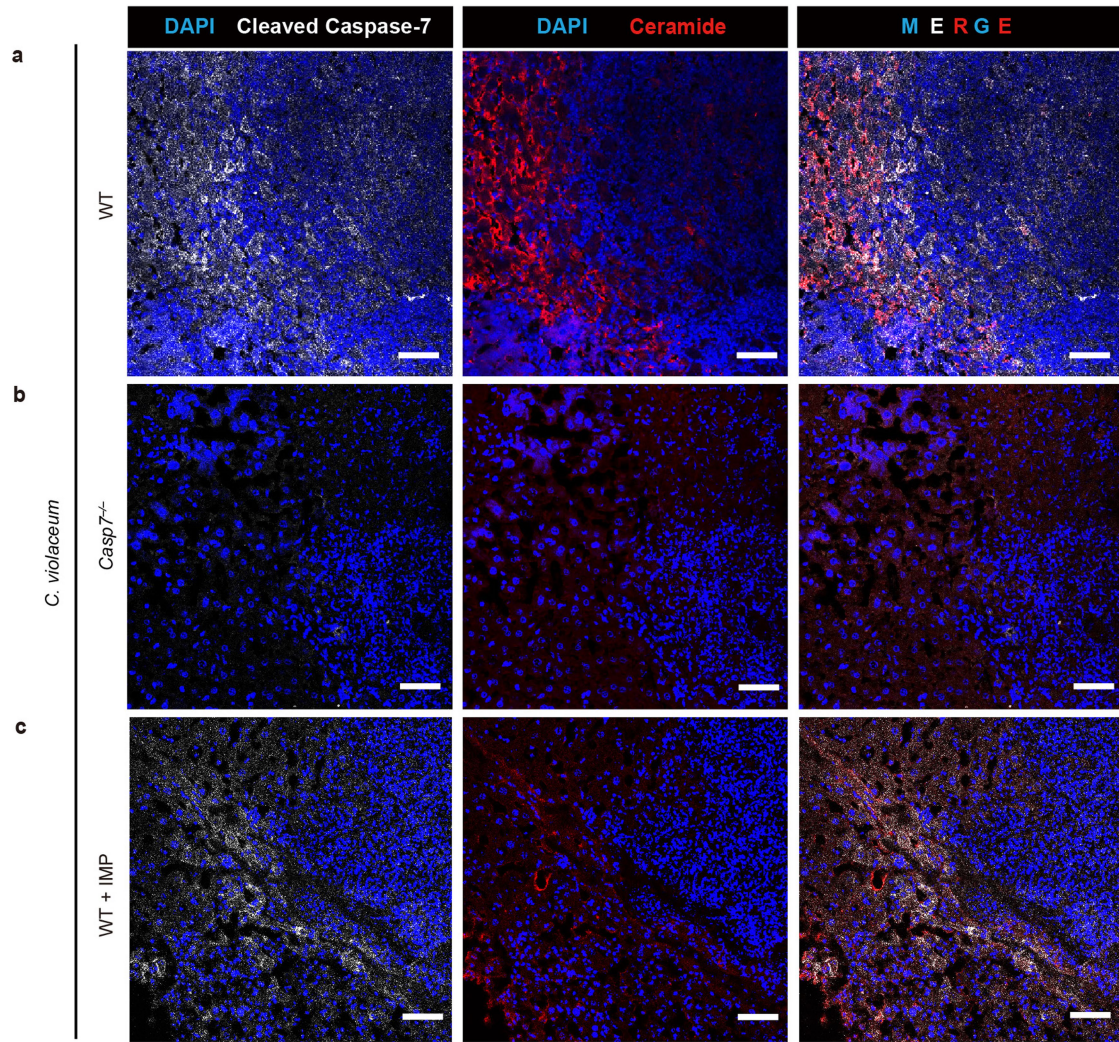


**Extended Data Fig. 10** | See next page for caption.

## Article

**Extended Data Fig. 10 | IL-18 primes NK cell cytotoxicity to activate caspase-7 in hepatocytes.** **a–b, e–g,** *Casp1-Il<sup>DKO</sup>* mice were infected with 10<sup>4</sup> *C. violaceum*, treated with PBS or IL-18 (1P0.2 µg recombinant mouse IL-18 (MBL) at day 0 and 1), and collected at 2 dpi. Livers were stained for the indicated markers via immunofluorescence. Single-channel zoom images are from inset box. Merged inset is shown in main Fig. 4f. Scale bars, 50 µm. **c**, Quantification of cleaved caspase-7 signal within lesions, with each dot as the average per mouse. **d**, Percent of cleaved caspase-7-positive cells that co-stain with CPS1. **g–j**, *Casp7<sup>-/-</sup>* or WT mice were left uninfected or infected with 10<sup>4</sup>

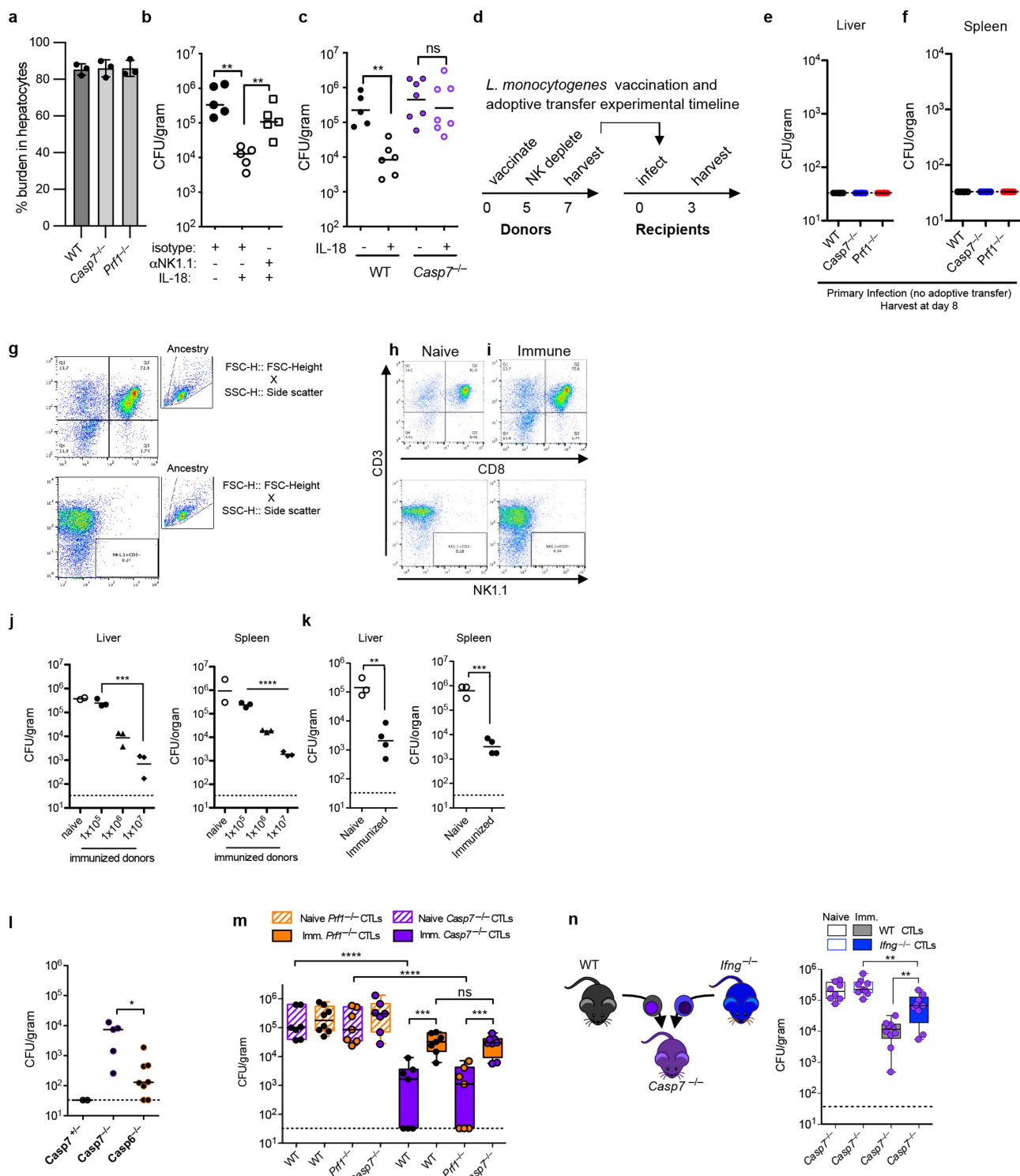
*C. violaceum* as indicated, and collected at 2 dpi. Representative images of livers stained for nuclei (DAPI; blue), cleaved caspase-7 (**g–h, j**, green), cleaved caspase-3 (**i**, red), TUNEL (**j**, red). **k–l**, WT mice were infected with 10<sup>4</sup> *C. violaceum* and collected at 3 dpi, then stained for cleaved caspase-7 (**k**, white), cleaved PARP (**l**, white). Scale bars, 50 µm. Data are pooled (**c–d**) or representative (**a–b, e–l**) of 2 experiments. \**P*<0.05, \*\**P*<0.01, \*\*\**P*<0.001, \*\*\*\**P*<0.0001 (Two-sided Mann–Whitney *U*-test). Bars indicate median values. Exact *p* and *n* values in Source Data EDF10.



**Extended Data Fig. 11 | Caspase-7 enhances ceramide production through ASM after NK-CTL attack.** a–c, Mice were treated with IMP or PBS, followed by intraperitoneal infection with  $10^4$  *C. violaceum* and collected at 3 dpi.

Representative images of infected livers from WT (a), Casp $7^{-/-}$  (b), or WT+IMP (c) mice stained for nuclei (DAPI; blue), cleaved caspase-7 (white), and ceramide (red). Scale bars, 50  $\mu$ m. Data are representative of 3 experiments.

# Article



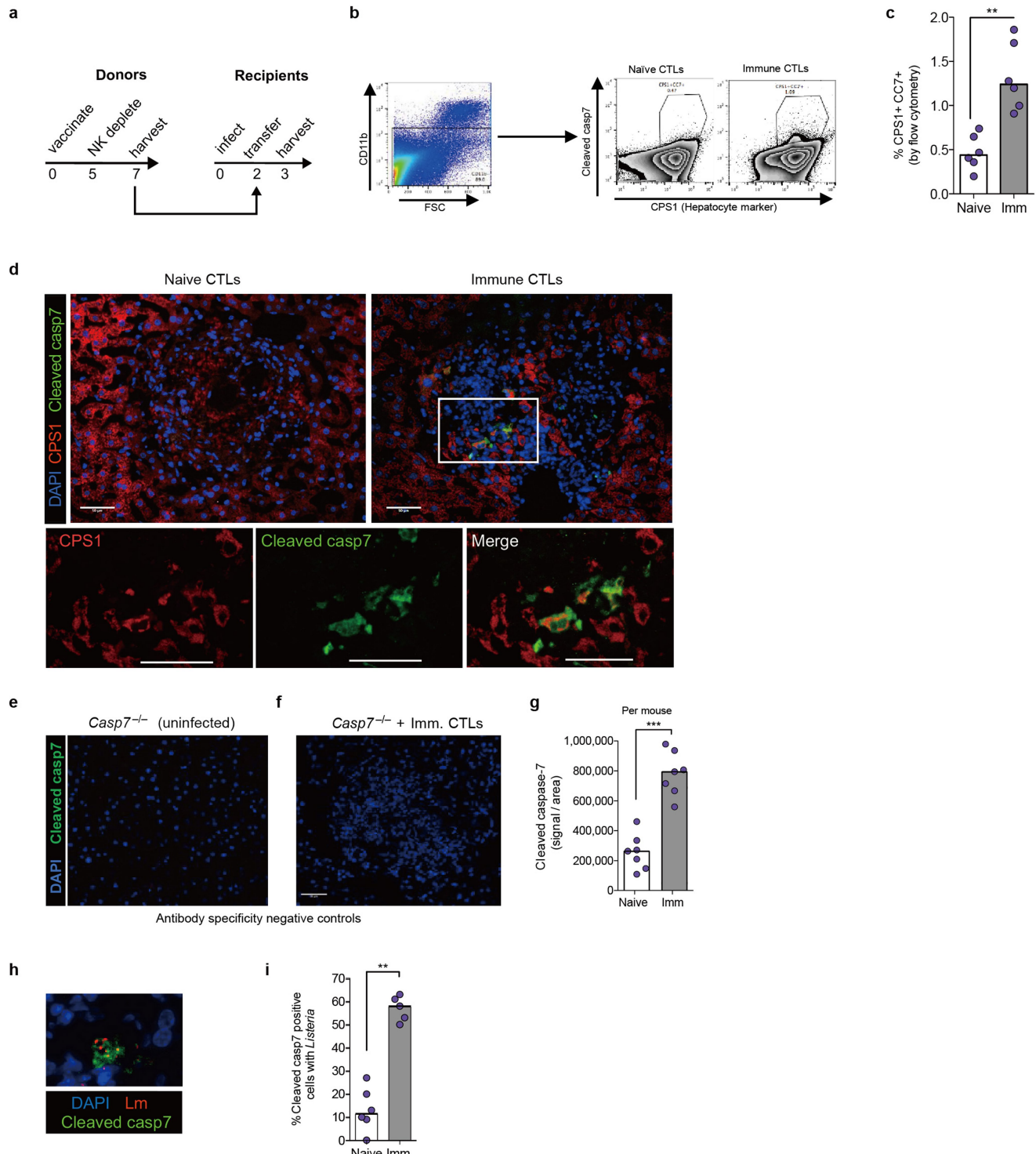
**Extended Data Fig. 12** | See next page for caption.

**Extended Data Fig. 12 | CTL transfer model during *L. monocytogenes***

**infection.** **a**, Percentage of bacterial burden localized to hepatocytes at 3 dpi. Equal weight liver sections were removed and the hepatocyte fraction was graphed as a percentage of the total burden by weight. 3 mice per genotype. **b–c**, Mice were infected IV with  $5 \times 10^3$  *L. monocytogenes* and IP treated with combinations of isotype antibody or NK depleting antibody (100 µg anti-NK1.1 PK136), with IL-18 (0.2 µg recombinant mouse IL-18) or isotype control as indicated. Mouse numbers (**b**) n = 5 each group; (**c**) WT PBS n = 6, WT IL-18 n = 6, *Casp7<sup>-/-</sup>* n = 7 each. **d**, Timeline for adoptive transfers. Donor mice were PBS treated (naïve) or vaccinated with  $1 \times 10^6$   $\Delta$ act*A*. *monocytogenes* (immune) in Fig. 5. **e–f**, Liver and splenic burdens 8 days post primary infection with  $5 \times 10^3$  *L. monocytogenes*. n = 6 mice each. **g**, Flow gating strategy for flow experiments depicted in (**h–i**). **h–i**, Donor mice were NK depleted (> 99% eliminated) and their CTLs enriched by negative selection (> 72% purity). **j**, Mice were adoptively transferred with the indicated numbers of purified CTLs (naïve were given  $1 \times 10^7$  as the maximum transferred number), infected with  $5 \times 10^4$  *L. monocytogenes* and bacterial burdens were analysed in the liver and spleen at 3 dpi. 2 naïve mice, 3 per immunized group. **k**, Bulk splenocyte transfer ( $5 \times 10^7$ , as previously described in<sup>23</sup>) with NK depletion was comparable to that of isolated CTLs. Naïve

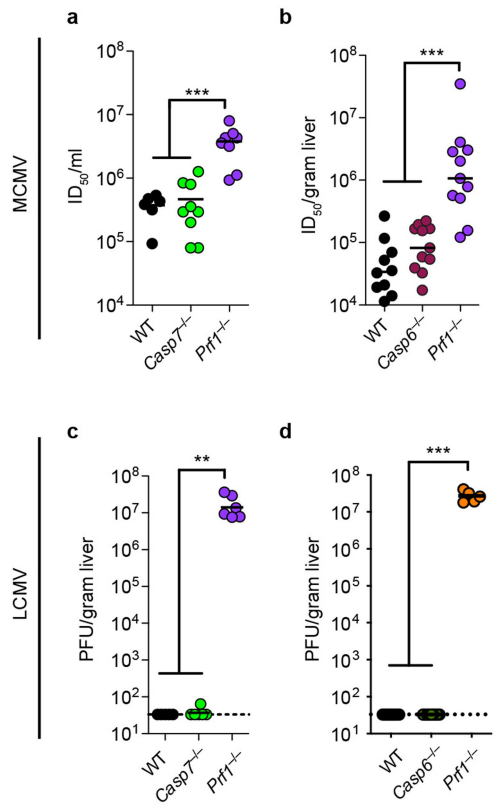
n = 3, immunized n = 4 mice. **l**, Mice were infected with  $5 \times 10^4$  of *L. monocytogenes* and adoptively transferred with immunized WT CTLs as in **d**. Liver bacterial burdens were determined at 3 dpi. Mouse numbers: *Casp7<sup>+/+</sup>* (n = 2F), *Casp7<sup>-/-</sup>* (n = 3M+2F), and *Casp6<sup>-/-</sup>* (n = 5F+3M). Note full clearance in *Casp7<sup>+/+</sup>* mice may be due to gender disparities or simply to low numbers leading to stochasticity and poor sampling. **m–n**, Donor mice were PBS treated (naïve) or vaccinated with  $1 \times 10^6$   $\Delta$ act*A*. *monocytogenes* (immune). (**m**) Adoptive transfer data from Fig. 5b,c are shown on the same graph, as all the transfers were done in the same 2 pooled experiments. Numbers of mice (**m**) WT mice with *Casp7<sup>-/-</sup>* CTLs n = 7 each, naïve *Prf1<sup>-/-</sup>* CTLs n = 8, immune *Prf1<sup>-/-</sup>* CTLs n = 7; naïve knockout recipients n = 7 each, immune recipients *Prf1<sup>-/-</sup>* n = 8, *Casp7<sup>-/-</sup>* n = 7; (**n**) naïve WT n = 8, immune WT n = 10, *Ifng<sup>-/-</sup>* n = 9 each. Data are representative of two experiments (**a, e–f, h**) or pooled from two experiments (**b–c, j–n**). \*P < 0.05, \*\*P < 0.01, \*\*\*P < 0.001, \*\*\*\*P < 0.0001 (Two-sided Mann–Whitney U-test) (**a–c, k, l**), or (**j, m, n**) one-way ANOVA with Tukey’s multiple comparison test. Bars indicate mean with standard deviation (**a**). Box plots show median, 25<sup>th</sup>–75<sup>th</sup> percentile, whiskers are minimum and maximum. Exact p and n values in Source Data EDF12.

# Article

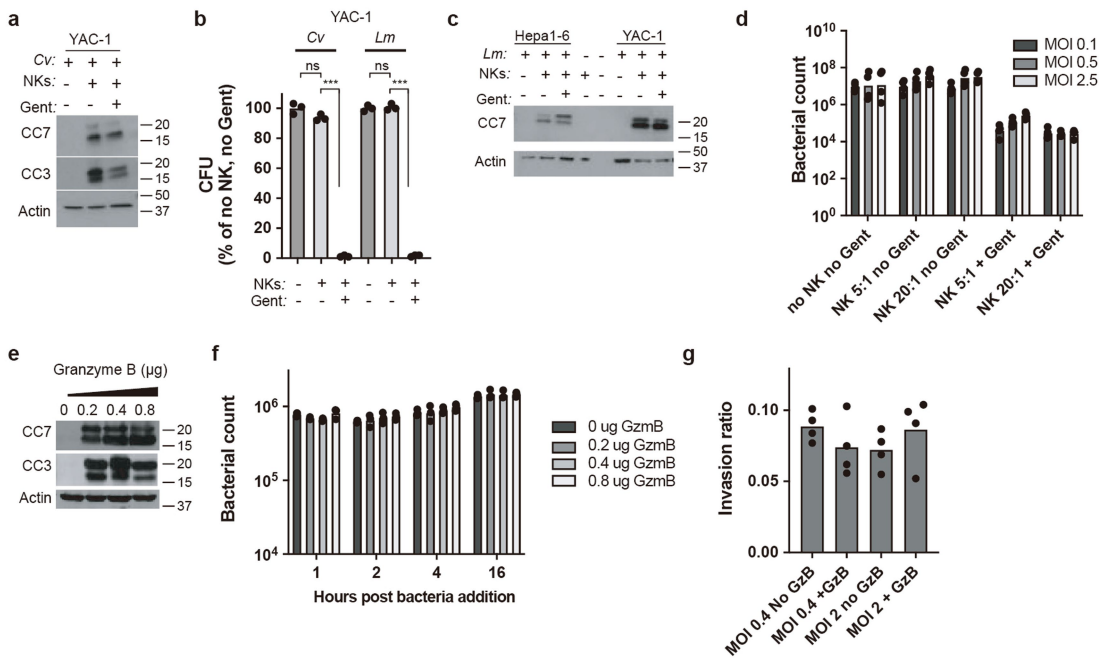


**Extended Data Fig. 13 | CTL transfer induces cleavage of caspase-7 during *L. monocytogenes* infection.** **a**, Timeline for adoptive transfers with recipients infected IV with  $5 \times 10^4$  *L. monocytogenes* in Extended Data Fig. 13. **b-c**, Flow cytometry of enriched hepatocytes for cleaved caspase-7 staining and gating scheme, with representative plot (**b**) and quantification of  $n = 6$  mice per group (**c**). **d**, Representative images of livers stained for nuclei (DAPI; blue), cleaved caspase-7 (green), and CPS1 (red). Scale bars, 50  $\mu$ m. **e-f**, Immunofluorescence control staining. *Casp7<sup>-/-</sup>* mice were left uninfected (**e**) or CTL transferred and infected with  $5 \times 10^4$  *L. monocytogenes* (**f**), and collected at 3 dpi. Representative

images of livers stained for nuclei (DAPI; blue) and cleaved caspase-7 (green). Scale bars, 50  $\mu$ m. **g**, Quantification of cleaved caspase-7 signal within lesions (dot = average per mouse;  $n = 7$  WT mice per group). **h-i**, Colocalization of cleaved caspase-7 signal and *L. monocytogenes* with representative image (**h**) and quantification (**i**) from  $n = 6$  naïve and  $n = 5$  immune WT mice. Scale bar, 50  $\mu$ m. Graphed data are pooled from 2 experiments (**c, g, i**). Images representative of 2 experiments (**d, h**) or one experiment (**e, f**). \* $P < 0.05$ , \*\* $P < 0.01$ , \*\*\* $P < 0.001$ , \*\*\*\* $P < 0.0001$  (Two-sided Mann–Whitney *U*-test). Bars indicate median values. Exact  $p$  and  $n$  values in Source Data EDF13.

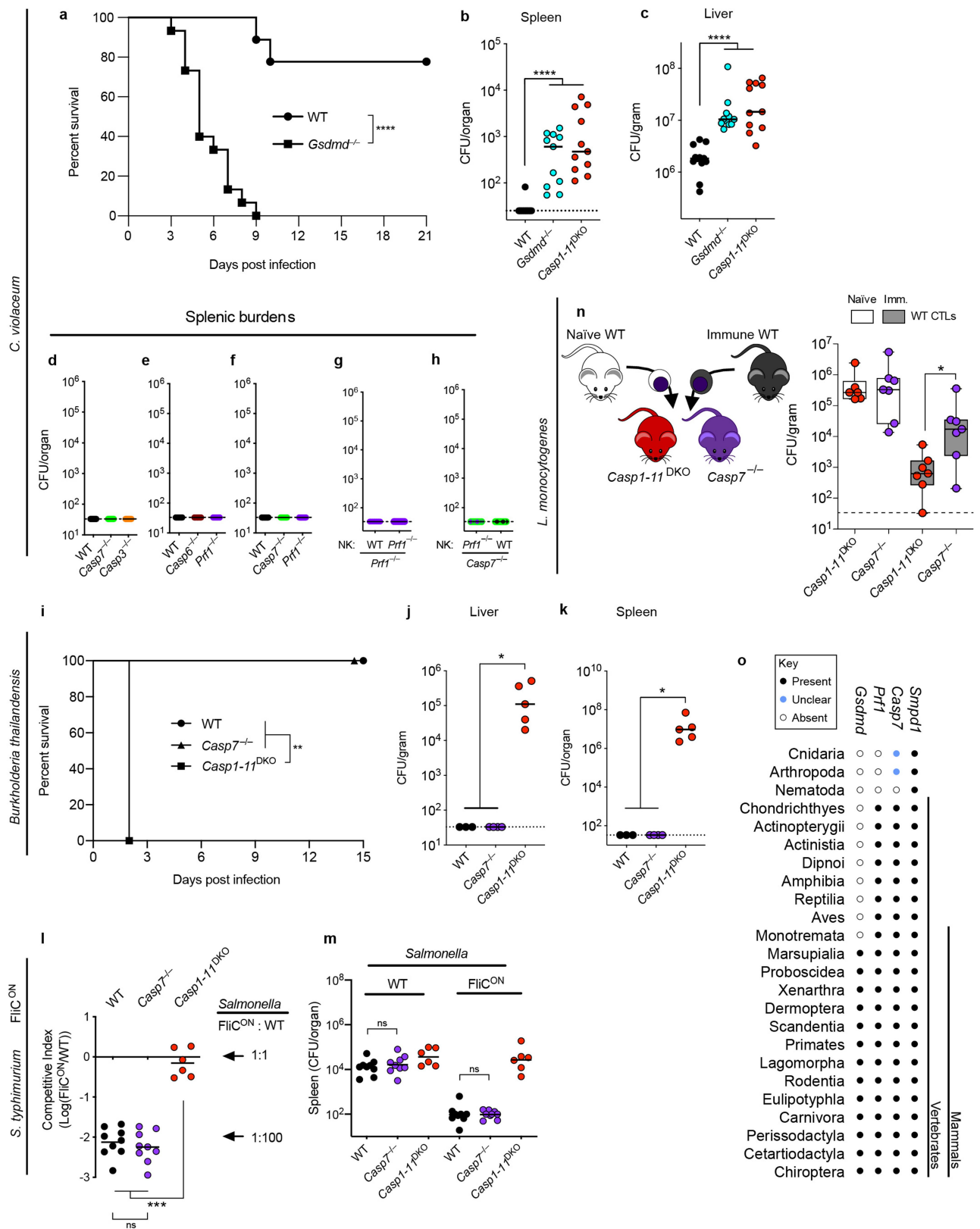


**Extended Data Fig. 14 | MCMV and LCMV are cleared independent of caspase-6 and caspase-7.** **a-b**, Mice were infected IP with  $5 \times 10^4$  PFU of MCMV. Viral titre in the liver was determined at 4 dpi from **(a)** n = 6 WT, n = 9 Casp7<sup>-/-</sup>, n = 8 Prf1<sup>-/-</sup>; **(b)** n = 10 WT, n = 11 Casp6<sup>-/-</sup>, n = 11 Prf1<sup>-/-</sup>. **c-d**, Mice were infected IP with  $2 \times 10^5$  PFU of LCMV. Viral titre in the liver was determined by plaque assay at 8 dpi from **(c)** n = 5 WT, n = 6 Casp7<sup>-/-</sup>, n = 6 Prf1<sup>-/-</sup>; **(d)** n = 8 WT, n = 9 Casp6<sup>-/-</sup>, n = 5 Prf1<sup>-/-</sup>. All data are pooled from 2 experiments. \*P < 0.05, \*\*P < 0.01, \*\*\*P < 0.001, \*\*\*\*P < 0.0001 (Two-sided Mann–Whitney U-test). Bars indicate median values. Exact p and n values in Source Data EDF14.



**Extended Data Fig. 15 | Granzyme B, active caspase-3 and active caspase-7 are not sufficient to kill bacteria in vitro.** a-d, NK co-culture killing assays (see “In vitro co-culture assays” in methods for detailed description) with *C. violaceum*-infected YAC-1 cells or *L. monocytogenes*-infected Hepa1-6 and YAC-1 cells as indicated. (a, c) Western blot analysis of cleaved caspase-3 (CC3) and/or cleaved caspase-7 (CC7). (b, d) Bacterial counts 5 h post co-culture.

e-f, Hepa1-6 cell lysates were spiked with granzyme B at the indicated amounts for 1 h and  $8 \times 10^6$  *L. monocytogenes* was added. Western blot analysis of CC3 and CC7 (e) and time course of bacterial numbers (f). g, Invasion assay with *L. monocytogenes* incubated in Hepa1-6 cell lysates for 16 h with granzyme B. All data are representative of 2 experiments. \* $P < 0.05$ , \*\* $P < 0.01$ , \*\*\* $P < 0.001$ , \*\*\*\* $P < 0.0001$  (Two-sided Mann–Whitney U-test). Bars indicate mean.



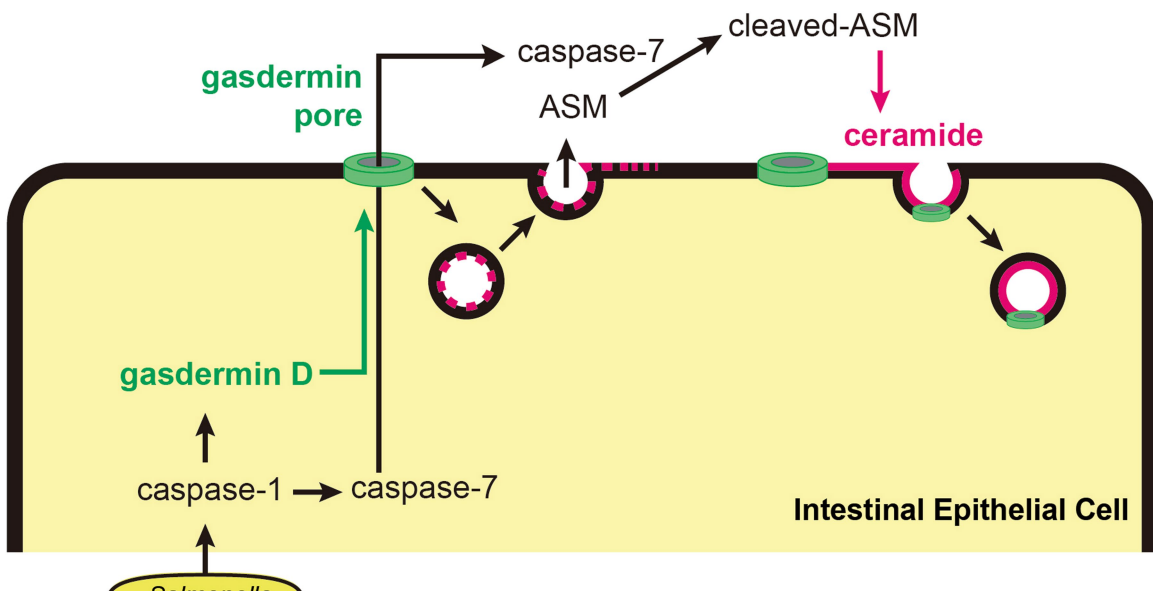
**Extended Data Fig. 16** | See next page for caption.

# Article

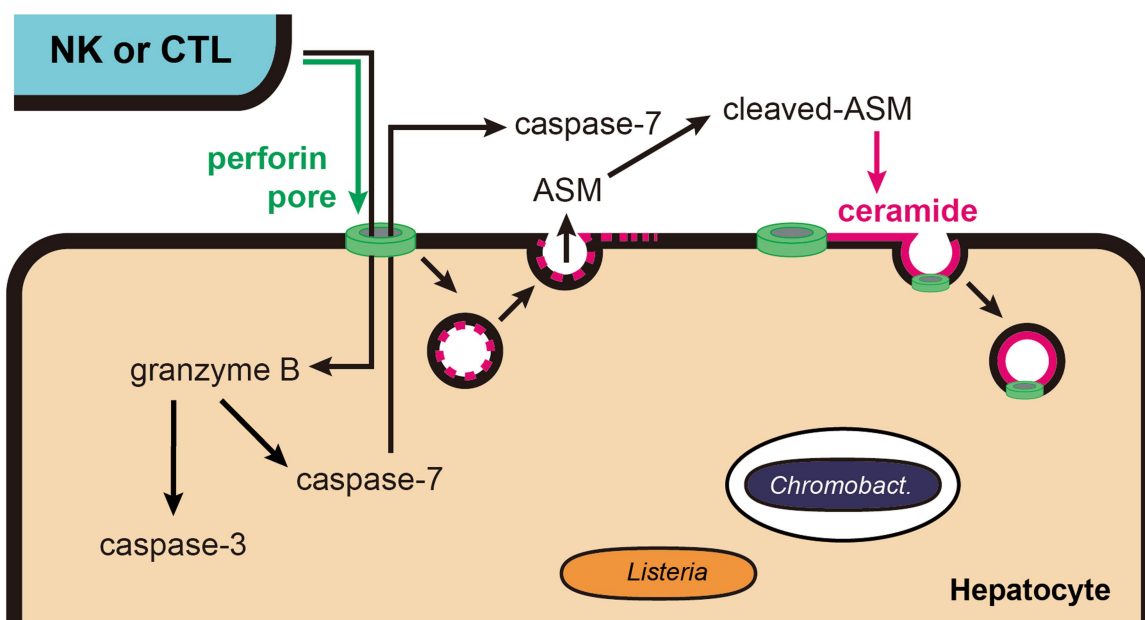
**Extended Data Fig. 16 | Pyroptotic activation of caspase-7 is not required for clearance of *C. violaceum*.** **a–c**, Mice were infected IP with  $1 \times 10^4$  *C. violaceum* and monitored for survival (**a**) or collected for bacterial counts at 2 dpi (**b–c**). **d–h**, Mice were infected with *C. violaceum* and spleen burdens determined 3 dpi; spleen burdens shown are from the same mice whose liver burdens are shown in Extended Data Fig. 9a, Fig. 4a,b, and Fig. 4d,e. **i–k**, Mice were infected IP with *B. thailandensis* at  $2 \times 10^7$  (**i**) or  $1 \times 10^4$  CFUs (**j–k**) and mice were monitored for survival (**i**) or bacterial burdens were enumerated 3 dpi (**j–k**). **l–m**, Mice were infected IP with  $1 \times 10^5$  total *S. typhimurium* ( $5 \times 10^4$  of WT plus  $5 \times 10^4$  of FliC<sup>ON</sup>), with bacterial burdens determined 2 dpi and burdens graphed as competitive index (CI) of FliC<sup>ON</sup> to WT bacteria (**l**) or graphed as total burdens (**m**). **n**, Liver bacterial burdens 3 dpi with  $5 \times 10^4$  *L. monocytogenes*, with adoptive transfer schematic. Donor mice were PBS treated (naïve) or vaccinated with  $1 \times 10^6$   $\Delta$ actA *L. monocytogenes* (immune). **O**, Presence or

absence of *Smpd1* (encoding ASM), *Casp7*, *Prf1*, and *Gsdmd* in the indicated taxonomic groups were determined by gene annotation and verified by reciprocal BLAST searches against the respective mouse gene product. Data are pooled from three experiments (**a–c**), pooled from two experiments (**d–h, l–n**) or representative of two experiments (**i–k**). Mouse numbers (**a**)  $n = 9$  WT,  $n = 15$  *Gsdmd*<sup>−/−</sup>; (**b–c**)  $n = 12$  WT,  $n = 11$  *Casp1*<sup>−/−</sup>*Casp11*<sup>−/−</sup>,  $n = 11$  *Gsdmd*<sup>−/−</sup>; (**i**)  $n = 5$  WT,  $n = 3$  *Casp1*<sup>−/−</sup>*Casp11*<sup>−/−</sup>,  $n = 5$  *Casp7*<sup>−/−</sup>; (**j–k**)  $n = 3$  WT,  $n = 4$  *Casp7*<sup>−/−</sup>,  $n = 5$  *Casp1*<sup>−/−</sup>*Casp11*<sup>−/−</sup>; (**l–m**)  $n = 9$  WT,  $n = 9$  *Casp7*<sup>−/−</sup>,  $n = 6$  *Casp1*<sup>−/−</sup>*Casp11*<sup>−/−</sup>; (**n**)  $n = 6$  naïve *Casp1*<sup>−/−</sup>*Casp11*<sup>−/−</sup>,  $n = 7$  immune *Casp1*<sup>−/−</sup>*Casp11*<sup>−/−</sup>,  $n = 7$  each *Casp7*<sup>−/−</sup>. \* $P < 0.05$ , \*\* $P < 0.01$ , \*\*\* $P < 0.001$ , \*\*\*\* $P < 0.0001$  (Two-sided Mann–Whitney *U*-test, or (**a, i**) log-rank Mantel–Cox test). Bars indicate median values. Box plots show median, 25<sup>th</sup>–75<sup>th</sup> percentile, whiskers are minimum and maximum. Exact  $p$  and  $n$  values in Source Data EDF16.

a



b



**Extended Data Fig. 17 | Model for membrane repair driven by caspase-7.**  
**a**, IECs detect the activity of the *Salmonella* T3SS via NLRC4 and activate caspase-1 in response. Caspase-1 then activates both the gasdermin D pore as well as caspase-7. We propose a model in which caspase-7 diffuses through the gasdermin D pore, thereby entering the extracellular space. Simultaneously, the gasdermin D pore triggers lysosomal exocytosis, thus delivering ASM to the extracellular space. In this model, caspase-7 and ASM meet in the extracellular space. Note that additional studies will be needed to validate the location of the caspase-7 and ASM interaction. Caspase-7 cleaves ASM,

increasing its enzymatic activity and generating more ceramide. This ceramide can then be used for continuous endocytic repair of gasdermin D pores to facilitate IEC extrusion. **b**, NK cells or CTLs attack by degranulating perforin and granzyme B. Perforin pores allow granzyme B to enter the target cell, where it activates caspase-3 (not shown) and caspase-7. Activated caspase-7 can exit the cell to encounter ASM, which generates ceramide that should allow endocytosis of perforin pores. We propose that this maintains cell integrity long enough for the cell to complete caspase-3-driven apoptosis.

## Reporting Summary

Nature Portfolio wishes to improve the reproducibility of the work that we publish. This form provides structure for consistency and transparency in reporting. For further information on Nature Portfolio policies, see our [Editorial Policies](#) and the [Editorial Policy Checklist](#).

### Statistics

For all statistical analyses, confirm that the following items are present in the figure legend, table legend, main text, or Methods section.

n/a Confirmed

- The exact sample size ( $n$ ) for each experimental group/condition, given as a discrete number and unit of measurement
- A statement on whether measurements were taken from distinct samples or whether the same sample was measured repeatedly
- The statistical test(s) used AND whether they are one- or two-sided  
*Only common tests should be described solely by name; describe more complex techniques in the Methods section.*
- A description of all covariates tested
- A description of any assumptions or corrections, such as tests of normality and adjustment for multiple comparisons
- A full description of the statistical parameters including central tendency (e.g. means) or other basic estimates (e.g. regression coefficient) AND variation (e.g. standard deviation) or associated estimates of uncertainty (e.g. confidence intervals)
- For null hypothesis testing, the test statistic (e.g.  $F$ ,  $t$ ,  $r$ ) with confidence intervals, effect sizes, degrees of freedom and  $P$  value noted  
*Give P values as exact values whenever suitable.*
- For Bayesian analysis, information on the choice of priors and Markov chain Monte Carlo settings
- For hierarchical and complex designs, identification of the appropriate level for tests and full reporting of outcomes
- Estimates of effect sizes (e.g. Cohen's  $d$ , Pearson's  $r$ ), indicating how they were calculated

*Our web collection on [statistics for biologists](#) contains articles on many of the points above.*

### Software and code

Policy information about [availability of computer code](#)

#### Data collection

microscopy or live imaging: MetaMorph 7.10  
flow cytometry: BD CellQuest Pro ver #5.2.1  
Confocal microscopy: ZEN Black Edition ver 14.0  
ELISA: Gen5 ver 3.10

#### Data analysis

microscopy: ImageJ ver 1.4.3.67, MetaMorph 7.10, ZEN Black Edition ver 14.0  
flow cytometry: FlowJo v10.3  
Graph generation and statistical analysis: GraphPad Prism v5 and v8 and Microsoft Excel 2013  
ELISA data: Gen5 ver 3.10 and Microsoft Excel 2013

For manuscripts utilizing custom algorithms or software that are central to the research but not yet described in published literature, software must be made available to editors and reviewers. We strongly encourage code deposition in a community repository (e.g. GitHub). See the Nature Portfolio [guidelines for submitting code & software](#) for further information.

## Data

Policy information about [availability of data](#)

All manuscripts must include a [data availability statement](#). This statement should provide the following information, where applicable:

- Accession codes, unique identifiers, or web links for publicly available datasets
- A description of any restrictions on data availability
- For clinical datasets or third party data, please ensure that the statement adheres to our [policy](#)

All relevant data are included in the Article or its Supplementary Information and Source Data files. More details are available from the corresponding authors upon request.

## Field-specific reporting

Please select the one below that is the best fit for your research. If you are not sure, read the appropriate sections before making your selection.

Life sciences       Behavioural & social sciences       Ecological, evolutionary & environmental sciences

For a reference copy of the document with all sections, see [nature.com/documents/nr-reporting-summary-flat.pdf](https://nature.com/documents/nr-reporting-summary-flat.pdf)

## Life sciences study design

All studies must disclose on these points even when the disclosure is negative.

Sample size	Target sample size was 6 mice per group based on power analysis and historical trends in data variance, however smaller or larger group sizes were used sometimes due to mouse availability. 6 mice are the preferred number to be used per group based on power analysis using the two tailed Student's t-test. The following parameters based on our prior experiments were used in power analysis (we use the website "Handbook of Biological Statistics, by John H. McDonald for reference). In a prior experiment that is typical of infection models in our lab, we find that the standard deviation for bacterial counts in WT infections is 1404 CFU (data is presented as log transformation; $\log(1404) = 0.17$ ). We assume the standard deviation for the test infection will be similar. We wish to detect differences with a p value of 0.05 (called alpha in the power analysis). The power of the experiment is the percent chance to find the indicated difference if it exists. We wish to have an 80 percent chance to find a 2 fold difference ( $\log_{10}(2) = 0.301$ ) and a 99% chance to detect a 3-fold difference in the CFU ( $\log_{10}(3) = 0.477$ ). We will have an equal number of mice in each group (sample size ratio N1 / N2). Key values in historical data that were used for this power analysis are as follows CFU/mg of spleen from a Salmonella infection: 4079, 6168, 3545, 5371, 1823, ,4963; average 4325; stdev 1404 (we use the log transformed data for the power analysis which are 3.61, 3.79, 3.55, 3.73, 3.26, 3.70; average 3.61; with a standard deviation of 0.17). The desired minimum difference for a 2 fold effect is 8650 (log transformed 3.94). However, when mouse numbers are limited, sometimes we use fewer mice, accepting that we may not detect more subtle differences between groups. When higher mouse numbers are available, we use larger numbers of mice to ensure detection of statistically significant differences.
Data exclusions	No data were excluded from analysis.
Replication	Every experiment was replicated at least in 2 separate cohorts, and in some up to 5 independent experiments. Only 6hpi and 15hpi EpCAM+ cell countin experiments were performed once as stated in Extended Data Fig. 1k-1l.
Randomization	All samples were allocated into experimental groups in a non-biased manner. Covariant controls are not relevant because we use inbred mice in all experiments. For mice, sexes were evenly distributed between groups.
Blinding	Experimental group assignments were not blinded because all mice are genetically identical (except for X and Y chromosomes, which were distributed equally between groups). DSS scoring and Salmonella pathology scoring were blinded.

## Reporting for specific materials, systems and methods

We require information from authors about some types of materials, experimental systems and methods used in many studies. Here, indicate whether each material, system or method listed is relevant to your study. If you are not sure if a list item applies to your research, read the appropriate section before selecting a response.

### Materials & experimental systems

n/a	Involved in the study
<input type="checkbox"/>	<input checked="" type="checkbox"/> Antibodies
<input type="checkbox"/>	<input checked="" type="checkbox"/> Eukaryotic cell lines
<input checked="" type="checkbox"/>	<input type="checkbox"/> Palaeontology and archaeology
<input type="checkbox"/>	<input checked="" type="checkbox"/> Animals and other organisms
<input checked="" type="checkbox"/>	<input type="checkbox"/> Human research participants
<input checked="" type="checkbox"/>	<input type="checkbox"/> Clinical data
<input checked="" type="checkbox"/>	<input type="checkbox"/> Dual use research of concern

### Methods

n/a	Involved in the study
<input checked="" type="checkbox"/>	<input type="checkbox"/> ChIP-seq
<input type="checkbox"/>	<input checked="" type="checkbox"/> Flow cytometry
<input checked="" type="checkbox"/>	<input type="checkbox"/> MRI-based neuroimaging

## Antibodies

### Antibodies used

Anti-cleaved caspase-7 (#9491, Cell Signaling), anti-cleaved caspase-3 (#9661, Cell Signaling), anti-GSDMD (ab209845, abcam), anti-EpCAM (BioLegend #118202, clone G8.8), anti-ceramide (1:200, ENZO Life Sciences #ALX-804-196 (clone MID 15B4)), and anti-ceramide (Glycobiotech #MAB\_0014, clone S58-9), GAPDH (#97166, Cell Signaling), anti-ASM (#PA-5 72432, Invitrogen), anti-caspase-1 p10 (M-20) (#sc-514, Santa Cruz Biotechnology), anti-caspase-9 (#9504, Cell Signaling), anti-cleaved caspase-8 (#8592, Cell Signaling), Phalloidin (1:1000, Invitrogen, # A12379, #A34055, #A22287), anti-rabbit (Cell Signaling #4412, #4414), anti-rat (Abcam #ab175475), anti-mouse; Invitrogen #A10037), anti-CPS-1 HRP (#198969, Abcam), anti-Listeria (#68592, Abcam), anti-cleaved-PARP-1 (D214) antibody (#STJ90100, St John's Laboratory), anti-CD45.2-PercPCy5.5 (104, Biolegend #109828), anti-NK1.1-FITC (PK136, Bioleged #108706), anti-CD8a (clone 53-6.7; Bioleged #109807).

Dilutions for antibodies are included in the Methods section of the manuscript.

### Validation

Cleaved caspase-7 antibody was validated using Casp7-knockout mice (immunofluorescence) and cells (western blot). Cleaved caspase-3 antibody was validated by using Casp3-knockout cells; further validated to not cross react with caspase-7 by using Casp7-/cells. Anti-GSDMD was validated by western blot with Gsdmd-knockout cells. Anti-EpCAM stains IECs specifically with the expected subcellular distribution; this antibody is extensively used to stain IECs, but was not further validated in our lab. Anti-ceramide antibody is validated using ceramide treated cells compared to untreated controls. Anti-GAPDH detected a band of the correct size, no further validation performed in our lab. Anti ASM was validated using HeLa cells that were CRISPR/Cas9 targeted for ASM and also Smpd1 DA/DA cells that lose the cleaved ASM band. Anti-caspase-1 validated by western with Casp1-knockout cells. Anti-caspase-9 detected a band of the correct size, and was validated to not cross react with caspase-7 using Casp7-knockout cells; no further validation performed in our lab; manufacturer states no cross reactivity with other caspases and shows apoptosis specific cleavage bands by western blot. Anti-caspase-8 detected a band of the correct size, and was validated to not cross react with caspase-7 using Casp7-knockout cells; no further validation performed in our lab; manufacturer states reactivity only to the cleaved caspase-8. Anti-CPS1 validated by manufacturer using western blot and immunohistochemical staining of liver, and stains liver cells of the correct size in our lab; this antibody is extensively used in histopathology of the liver, but was not further validated in our lab. Anti-Listeria antibody is validated by staining only to bacteria sized and shaped objects, and not staining outside the infected lesions (lesions were identified by DAPI). Anti-cleaved PARP1 antibody validated by not staining to healthy tissue outside the infected lesions. Anti CD45.2 is stated by the manufacturer web site to be specific and not react with CD45.1; further validation not performed in our lab. Anti NK1.1 is stated in the manufacturer web site that each lot is "quality control tested by immunofluorescent staining with flow cytometric analysis"; it was not further validated in our lab. Anti CD8a is stated in the manufacturer web site to block antigen presentation via MHC class I and inhibit T cell responses to IL-2, along with other validation statements, implying the specific binding to CD8; it was not further validated in our lab.

## Eukaryotic cell lines

### Policy information about [cell lines](#)

#### Cell line source(s)

L-WRN cells (ATCC #3276) was purchased from ATCC.

HeLa cell line was purchased from Duke University Cell Culture Facility, who obtained them from ATCC.

Hepa1-6 cells (ATCC CRL-1830) were purchased from ATCC.

YAC-1 cells (ATCC TIB-160) were purchased from ATCC.

#### Authentication

L-WRN cells were purchased directly from ATCC, which is considered a reputable vendor; they were further authenticated by their phenotype of supporting organoid growth, a property that other cell lines cannot accomplish. HeLa cells were purchased from Duke University Cell Culture Facility, and were authenticated by Short Tandem Repeat (STR) analysis performed by this facility. Hepa1-6 and YAC-1 were purchased directly from ATCC, which is considered a reputable source. Hepa1-6 cells were partially authenticated by visual morphology. YAC-1 cells were partially authenticated by the phenotype of being attacked by NK cells. Cell lines were not further authenticated.

#### Mycoplasma contamination

The cells were tested negative for mycoplasma.

#### Commonly misidentified lines (See [ICLAC](#) register)

No commonly misidentified cell lines were used.

## Animals and other organisms

### Policy information about [studies involving animals; ARRIVE guidelines](#) recommended for reporting animal research

#### Laboratory animals

The previously generated mouse lines (listed below) were used in this study: wild type (WT) C57BL/6, , Prf1 null mice, Casp6 null mice, Casp7 null mice, Casp3 null mice, Gsdmd null mice, Casp1 null Casp11 null mice, NLRC4 null mice. This study generated Smpd1 mutant (D249A/D249A) mice. All strains were maintained in C57BL/6 background. For mouse infections, 8-12-week-old mice were used. All strains were maintained on 12/12 light cycles, at 72 +/- 2 °F, and under the humidity set point of 45%. Male and female mice were used in equivalent numbers unless otherwise indicated.

#### Wild animals

No wild animals were used.

#### Field-collected samples

No field-collected samples were used.

#### Ethics oversight

Animal protocols were approved by the Institutional Animal Care and Use Committee at the University of North Carolina at Chapel Hill, or by the Institutional Animal Care and Use Committee at Duke University and met guidelines of the US National Institutes of Health for the humane care of animals.

Note that full information on the approval of the study protocol must also be provided in the manuscript.

# Flow Cytometry

## Plots

Confirm that:

- The axis labels state the marker and fluorochrome used (e.g. CD4-FITC).
- The axis scales are clearly visible. Include numbers along axes only for bottom left plot of group (a 'group' is an analysis of identical markers).
- All plots are contour plots with outliers or pseudocolor plots.
- A numerical value for number of cells or percentage (with statistics) is provided.

## Methodology

### Sample preparation

A detailed description is available in the "Liver cell enrichment" section of the Methods. In brief, mouse livers were harvested, perfused with collagenase type I, finely cut, and incubated to allow collagenase to liberate cells. The pieces were then mashed through a cell strainer, washed, and spun several times at 50 x g to separate hepatocytes from immune cells. Cells were subjected to RBC Lysis Buffer to remove contaminating red blood cells before they were stained.

### Instrument

FACSCalibur

### Software

BD CellQuest Pro was used to collect the samples. Data was analyzed in FlowJo.

### Cell population abundance

Hepatocytes represented >96% of the cells run on the FACSCalibur. This was determined via CPS1 staining, which is specific to hepatocytes and not present in the immune cell fraction.

### Gating strategy

An example of the gating strategy is present in Extended Data Figure 6a. This shows that CD11b was used as a dump gate to eliminate residual immune cells from the analyses regarding hepatocytes. In Extended Data Figure 5d, lymphocyte population gates in normal FSC/SSC axis were used for further analysis of NK cell and CD3+CD8+ T cell populations.

- Tick this box to confirm that a figure exemplifying the gating strategy is provided in the Supplementary Information.